UCRL- 95218 Rev. 1
PREPRINT

Neoclassical Transport in Stellarators

Darwin D-M. Ho
Lawrence Livermore National Laboratory
Russell M. Kulsrud
Plasma Physics Laboratory, Princeton University

This paper was prepared for submittal to
Physics of Fluids

August 20, 1986

DISCLAIMER

NEOCLASSICAL TRANSPORT IN STELLARATORS

Darwin D.-M. Ho
Lawrence Livermore National Laboratory, University of California,
Livermore, California 94550
Russell M. Kulsrud
Plasma Physics Laboratory, Princeton University,
Princeton, New Jersey 08544

ABSTRACT

The stellarator neoclassical transport due to particles trapped in local helical wells is calculated in the low-collisionality regime using a systematic expansion. The behavior of electron transport is found to be the same over a wide range of energies but the behavior of ion transport for low energy ions is found to be different than that for high energy ions. Furthermore, the electron fluxes do not vary with the change in the radial ambipolar electric field nearly as much as do the ion fluxes. Thus, the particle diffusion is controlled by the electrons. A non-radial ambipolar electric field is induced by ion-drift. This electric field enhances the transport by about 15 - 20%. A convenient graphical method that allows one to determine the magnitude of the radial ambipolar field for machines with different parameters is presented. Numerical examples show that electron energy confinement time is comparable to the ion energy confinement time for all the different size stellarators studied. Although the neoclassical losses are large, it is shown that ignition can be achieved in a reasonably sized stellarator reactor. Finally, from the standpoint of reactor economics, the confinement scaling law shows that in order to increase $n\tau$, it is better to increase the aspect ratio than the overall dimensions of the reactor.

I. INTRODUCTION

In recent years, there has been renewed interest in stellarator physics because of encouraging experimental and theoretical results.[1,2] Experimental results from the Wendelstein VII-A and Heliotron E stellarators[3,4] have shown that the energy confinement time is longer than the confinement time of tokamaks scaled to a comparable size with the same toroidal magnetic field strength. Theoretical studies using three-dimensional computer codes have indicated that stable stellarator operation is possible for plasma β's between 10 to 20%.[5,6] Stellarators have another attractive feature of being able to operate without a toroidal current. Besides providing steady-state operation, the current-free nature of the stellarator should avoid major disruptions. These advantages make the stellarator an attractive candidate for a future high performance reactor.

On the other hand, stellarators have a major drawback. This arises from the fact that the external helical windings produce local magnetic wells (henceforth, these local magnetic wells are referred to as helical wells) in which trapped particles are badly confined. This is a direct consequence of the lack of toroidal symmetry. The enhanced transport produced by particles trapped in helical wells can be as much as two orders of magnitude larger than the (neoclassical) transport produced by particles on banana orbits in a tokamak. The enhanced transport is strongest in the high-temperature, low-collisionality regime. This is the regime in which a trapped particle can bounce many times in a helical well before it detraps by collisions, and it is also the regime in which reactors are likely to operate. Thus, the nature of neoclassical transport resulting from nonaxisymmetry plays a critical role in determining the confinement in stellarator reactors.

Various authors have analyzed the transport problem in a nonaxisymmetric torus. A brief, but by no means complete, review of the previous studies is given here. Analytical studies carried out by Frieman[7] and by Connor and Hastie[8] showed that the diffusion coefficient is inversely proportional to the collision frequency ν, but they did not correctly include the important effect caused by an ambipolar radial electric field on ion transport. Galeev et al.,[9] using a variational principle, and Galeev and Sagdeev,[10] using an expansion technique, showed that the ambipolar field reduces the ion diffusion coefficient, but they did not investigate the ion behavior over a wide energy range and other effects. Extending Galeev's work, Mynick[11] studied the effect on transport of a new non-radial ambipolar electric field. This electric field is generated by ion drift and has a component tangential to magnetic surfaces. Boozer and Kuo-Petravic[12] evaluated the diffusion coefficient using a Monte-Carlo technique. In their work, however, the effect of the self-consistent ambipolar electric field on transport was not discussed in detail. The Monte-Carlo technique used in the ATF report[13] to estimate the plasma confinement time did not include the diffusion due to a temperature gradient. Kovrizhnykh has written an extensive review of all transport processes in nonaxisymmetric devices[14] and has applied these results to various stellarators.[15] He found that in some cases electron transport is the main loss process in stellarators.

From the above review, it can be seen that the physics of transport in stellarators is complex and that it is not clear whether all the important physics have been correctly included. Because of the renewed interest in stellarator physics and the importance of the neoclassical transport in stellarators, it is now appropriate to establish a systematic treatment that can include all the essential physics in stellarator transport. In this paper, the complex stellarator magnetic field is replaced by a simplified model field that has local magnetic wells. In addition, the use of a systematic expansion technique allows the transport calculation to be treated analytically. From this systematic analysis, previous results are recovered in a natural way, and new transport phenomena are uncovered. Although the calculations given here do not yield a precise confinement time for a real machine geometry, they do indicate that the inclusion of various new effects and the diffusion due to a temperature gradient can increase the estimate of transport by a factor as large as three (e.g., compared to a Monte-Carlo calculation without the inclusion of a temperature gradient). Therefore, it is necessary to treat the physics more precisely.

The results from the analysis in this paper show that for most stellarators, electron flux is relatively insensitive to variations in the ambipolar electric field. In contrast, the ion flux depends sensitively on the electric field variations. Thus, the particle transport is governed by electron diffusion and a good estimate of the total particle transport can be obtained from electron diffusion without knowing the exact value of the ambipolar field. The nonradial ambipolar field caused by ion drift enhances the transport by about 15 - 20%. Electrons with five to six times the thermal energy give the dominant contribution to electron transport. The effect of collisionless detrapping/entrapping on ion transport becomes important only when ion energy is above the energy range (three to four times the thermal energy) that gives the dominant contribution to ion diffusion. Numerical examples show that the electron energy confinement time is approximately equal to that of the ions for machines with different sizes and plasma temperatures. Furthermore, it is shown that the ignition condition can be achieved if the machine size is reasonably large.

In many ways, the calculations and results of the electron and ion diffusion coefficents presented in Secs. IV B and IV C are similar to those of Galeev and Sagdeev.[10] However, our presentation is more detailed and rigorous than theirs. The ion diffusion coefficient given in this paper is smaller than that in Ref. 10 by a factor of five after the numerical integration for the proper energy weighting of the Maxwellian distribution function is carried out correctly.

This paper is organized as follows: The simplified magnetic field geometry is described in Sec. II. A heuristic derivation of the transport coefficients in the low-collisionality regime is presented in Sec. III. The formal analysis starts in Sec. IV. The expansion and solubility conditions for the drift-Boltzmann equation are discussed, and a set of reduced equations for trapped and untrapped particles is obtained in Sec. IV A. The electron distribution function satisfying the reduced equations is obtained in Sec. IV B by a second expansion. Electron fluxes are also given in this section. The calculation for ion transport is presented in Sec. IV C. The effect of the non-radial electric field caused by ion drift on transport is examined in Sec. IV D. In Sec. V a convenient graphical method for determining the self-consistent radial ambipolar electric field is presented, and the scaling laws for confinement are given. Finally, the results are summarized, and their significance for stellarator reactors is discussed in Sec. VI. Appendix A presents the bounce-average calculation for the collision operator. The heuristic derivation of the ion diffusion coefficient with the effect of collisionless detrapping and entrapping is presented in Appendix B. Because of its length, this paper has been written in a concise manner. The interested readers are referred to Refs. 16 and 17 for detailed derivation of some of the equations appeared in this paper.

Only neoclassical transport has been addressed in this paper; however, convective transport may be present in a reactor since reactors should operate at the highest possible plasma β in order to give the maximum output power. As a consequence, the β may exceed the critical β limit by a small amount in some regions of the plasma, and this gives rise to pressure-driven convective cells. Thus, the transport in these regions is governed by both neoclassical and convective transport. Such convective transport has been studied by Ho and Kulsrud in Ref. 18 and by Connor et al. in Ref. 19.

II. MAGNETIC FIELD GEOMETRY

In order to allow the analysis to be carried out analytically, the magnetic surfaces are assumed to be nested circular tori. The simplified magnetic field strength, which has features in common with a general stellarator field, is approximated by

$$B = B_0 \left[1 - \epsilon_h(r) \cos(\ell\theta - m\zeta) - \epsilon_t \frac{r}{a} \cos\theta\right] \quad . \tag{1}$$

Here, ℓ is the multipolarity, m is the number of field periods, ϵ_t is the inverse aspect ratio (a/R_0), and ϵ_h is the depth of the helical wells caused by the externally imposed helical windings. The toroidal coordinate system, in terms of minor radius r, poloidal angle θ, and the toroidal angle ζ is shown in Fig. 1.

The first and the third term in the above expression represent the toroidal magnetic field which decreases as the major radius $R = R_0 + r \cos\theta$ increases. The toroidal field gradient results in a grad-B drift of electrons and ions, which is parallel to the major axis. If the toroidal magnetic field points in the direction of increasing ζ, then the electron grad-B drift is toward the upper region $(0 \leq \theta \leq \pi)$ of the torus and the ion grad-B drift is toward the lower region $(\pi \leq \theta \leq 2\pi)$ of the torus. The second term in Eq. (1) describes the magnetic field variation due to the helical wells (see Fig. 2). It is this term that destroys the toroidal symmetry. Particles trapped in local helical wells have a grad-B drift component that is normal to the magnetic surface and this produces the major contribution to diffusion in a stellarator.

III. HEURISTIC DERIVATION OF COLLISIONAL DIFFUSION COEFFICIENTS

Qualitative physical arguments are used in this section to obtain the collisional diffusion coefficients in the low- collisionality regime. The electron and ion diffusion coefficients are obtained by using the classical random-walk formula

$$D \sim \Delta^2 \bar{\nu} F \quad , \tag{2}$$

where Δ is the step-size, $\bar{\nu}$ is the characteristic frequency of taking a step in the random-walk process, and F is the fraction of particles participating in the diffusion process.

Rigorous kinetic theory is applied in Sec. IV to calculate the exact expression for the diffusion coefficients.

A. Electron Diffusion Coefficient

Electrons trapped in local helical wells (henceforth, unless specified, trapped particles mean trapped in helical wells) drift away from their initial magnetic surfaces due to the toroidal grad-B drift. Coulomb collisions with other particles can convert a trapped electron into an untrapped one. This untrapped electron can become trapped again, through further collisions, at any arbitrary poloidal location on the magnetic surface. Thus, electrons random-walk away from their initial magnetic surface with step-size

$$\Delta \sim \frac{v_B}{\nu_{eff}} \quad .$$

Here, v_B is the grad-B drift velocity, and ν_{eff} is the effective collision frequency, i.e., the frequency for scattering across the trapping region in velocity space (see Fig. 3). Note that ν_{eff} is equal to ϵ_h^{-1} times the electron collision frequency ν_e (which is the reciprocal of the 90° "deflection time"[20]). The characteristic frequency for electrons to take a step is also ν_{eff}. Only the trapped electrons, the fraction of which is proportional to $(\epsilon_h)^{1/2}$, participate in this diffusion process. Thus, by Eq. (2), the diffusion coefficient for electrons is

$$D_e \sim \frac{v_B^2}{\nu_{eff}} \epsilon_h \quad . \tag{3}$$

Because the trapped region in velocity space is small, $mv^2/2 \approx \epsilon > mv_\parallel^2/2$ for trapped particles. Here ϵ is the particle energy. Hence,

$$|v_B| \cong \frac{c\epsilon}{eB_0R_0} \quad .$$

Using this approximation and noting that $\nu_e \propto n\epsilon^{-3/2}$, Eq. (3) shows that $D_e \propto \epsilon^{7/2} n^{-1}$. The large ϵ dependence indicates that the high energy electrons give the dominant contribution to diffusion. Note that although $D_e \propto n^{-1}$, the electron flux is roughly independent of density since the flux is proportional to $D_e(\partial n/\partial r)$. Also note that the helical field gradient also results in a grad-B drift. However, the drift component that is normal to a magnetic surface is zero after bounce averaging [see Eq. (19)].

B. Ion Diffusion Coefficient

In the absence of an ambipolar electric field, the ion diffusion coefficient D_i is obtained by replacing ν_e in Eq. (3) by ν_i. This value of D_i for a deuteron is approximately sixty times larger than D_e because the large deuteron to electron mass ratio yields a deuteron collision frequency about sixty times smaller than that of the electrons while v_B is the same size. Thus, a radial electric field E_r must arise to reduce the ion flux to the same level as the electron flux in order to preserve quasineutrality. This ambipolar electric field reduces the step-size for ion diffusion by changing the ion orbits. The $\vec{E}_r \times \vec{B}$ drift causes particles to rotate poloidally. In general, $|E_r|$ is strong enough to ensure that all the trapped ions, except those with low energy (less than thermal energy), can experience several poloidal rotations before becoming detrapped. (Most trapped electrons, however, cannot make a full poloidal rotation before they are detrapped by collisions since $\nu_e \gg \nu_i$.) Superposition of the grad-B drift upon the poloidal drift results in an outward shift of the center of the trapped-ion drift orbit from the center of the magnetic surface (see Fig. 4) by a distance

$$\Delta \equiv \frac{v_B}{\Omega_E} \quad .$$

Here,

$$\Omega_E \equiv \frac{c\vec{E}_r x\vec{B}}{rB^2} \quad ,$$

is the poloidal rotation frequency of the trapped ions. The shift Δ is the random-walk step-size for ions.

To zeroth order in ϵ_h, the grad-B drift velocity of trapped ions is independent of their pitch angle. Consequently, the shift Δ is the same for all trapped ions, and they do not experience any random-walk until they leave the trapped region. Therefore, the dominant contribution to ion diffusion arises from the barely trapped ions. The characteristic time for a barely trapped ion to detrap through collisions is $\underline{O}(\Omega_E^{-1})$. The fraction of ions in the barely trapped region in velocity space that can become detrapped in the time Ω_E^{-1} is $O(\nu_i/\Omega_E)^{1/2}$. Thus, from Eq. (2), the diffusion coefficient for ions is [16]

$$D_i(\epsilon) \sim \frac{v_B^2}{\Omega_E}\left(\frac{\nu_i}{\Omega_E}\right)^{1/2} \quad . \tag{4}$$

The $\Omega_E^{-3/2}$ dependence indicates that the effect of the electric field in changing the ion orbits is very efficient in reducing the ion diffusion. In addition, ion mobility in E_r reduces the ion flux somewhat further. (See the expressions for the ion particle and energy fluxes given in Sec. IV C.)

If the helical well depth ϵ_h varies with minor radius, then ions can collisionlessly detrap out of and entrap into helical wells. This effect is discussed in Appendix B.

IV. FORMAL ANALYSIS OF COLLISIONAL TRANSPORT

A. Expansion and the Solubility Conditions for the Drift-Boltzmann Equation

Plasmas in some of the recent experimental stellarators and in stellarator reactors (see Table I) are in the long-mean-free path regime; furthermore, the characteristic length and plasma confinement times in transport studies are long compared to particle gyroradii and gyroperiods, respectively. Therefore, it is appropriate to use the drift-Boltzmann equation[21,22] to study collisional diffusion. If the magnetic field is time independent, the drift-Boltzmann equation has the form

$$\frac{\partial f_p}{\partial t} + (\vec{v}_\parallel + \vec{v}_D) \cdot \vec{\nabla} f_p + e_p \frac{\partial \Phi}{\partial t} \frac{\partial f_p}{\partial \epsilon} = C(f_p, f) \quad , \tag{5}$$

where the guiding-center distribution function of species p is

$$f_p = f_p(\epsilon, \mu, \vec{r}, t) \quad ,$$

the particle energy is

$$\varepsilon = \frac{m_p v^2}{2} + e_p \Phi \quad ,$$

the magnetic moment is

$$\mu = \frac{m_p v_\perp^2}{2B} \quad ,$$

and the position vector r is in (r,θ,ζ) coordinates. Each of the partial derivatives in Eq. (5) is performed by holding five of the six independent variables $\varepsilon,\mu,\vec{r},t$ constant.

The drift velocity $\vec{v}_D$ is the part of the guiding-center velocity that is perpendicular to the line of force:

$$\vec{v}_D = \frac{m_p c}{e_p B} \left(\frac{v_\perp^2}{2} + v_\parallel^2\right) \frac{\vec{B}\times\vec{\nabla}B}{B^2} + c\,\frac{\vec{B}\times\nabla\Phi}{B^2} \quad . \tag{6}$$

Inserting the expression for the magnetic field, Eq. (1), into the above equation, the radial and poloidal components of $\vec{v}_D$ are

$$\vec{v}_D \cdot \hat{e}_r = \frac{(\mu + m v_\parallel^2/B)B_0}{m_p \omega_p R_0}\left[\sin\theta + \frac{\ell \varepsilon_h}{(r/R_0)} \sin(\ell\theta - m\zeta)\right] + \frac{c}{B}\frac{1}{r}\frac{\partial\Phi}{\partial\theta} \quad ,$$

$$\vec{v}_D \cdot \hat{e}_\theta = \frac{(\mu + m v_\parallel^2/B)B_0}{m_p \omega_p R_0}\left[\cos\theta + \frac{\ell \varepsilon_h}{(r/R_0)} \cos(\ell\theta - m\zeta)\right] + \frac{c}{B}\frac{\partial\Phi}{\partial r} \quad , \tag{7}$$

where $\omega_p \equiv e_p B/m_p c$.

In the low-collisionality limit, the collision frequency ν and the effective collision frequency ν_{eff} are small compared to the respective trapped and untrapped particle bounce frequency ω_b. For untrapped particles, this limit can be expressed as

$$\nu \ll \omega_b \text{ (untrapped)} \sim \frac{v_\parallel}{qR} \quad , \tag{8a}$$

where qR is the connection length with q the inverse of the normalized rotational transform ι. The corresponding condition for helically trapped particles is

$$\nu_{eff} \ll \omega_b \text{ (trapped)} \sim \frac{(\varepsilon_h)^{1/2} v_\parallel}{L} \quad , \tag{8b}$$

where L is the distance between two helical mirror points. As an example, using the parameters for the reference stellarator (see Table I) with m = 6, $\nu_{eff} \approx 8.5 \times 10^4\ \sec^{-1}$ ($1.4 \times 10^3\ \sec^{-1}$) and $\omega_b \approx 10^6\ \sec^{-1}$ ($10^4\ \sec^{-1}$) for electrons (ions). Further, in one bounce period, a particle only drifts a tiny distance away from a magnetic surface, i.e.,

$$\frac{v_D}{a} \ll \omega_b \quad . \tag{9}$$

For both electrons and ions, $v_B/a \approx 10^2\ \sec^{-1}$ for the reference stellarators. Using the machine parameter given in Table I, it can be shown that inequalities (8) and (9) are indeed valid.

Inequalities (8) and (9) suggest solving Eq. (5) by expanding f_p in terms of $1/v_\parallel$:

$$f_p = F_{p0} + F_{p1} + F_{p2} + \ldots \quad . \tag{10}$$

Equation (5) to lowest order is

$$\vec{v}_\parallel \cdot \vec{\nabla} F_{p0} = 0 \quad . \tag{11}$$

This implies that F_{p0} is constant along a line of force. For the untrapped particle distribution function $f_p^{U.T.}$, Eq. (11) implies

$$F_{p0}^{U.T.} = F_{p0}^{U.T.}(\varepsilon,\mu,r,t) \quad . \tag{12}$$

Note that $F_{p0}^{U.T.}$ is independent of θ.

Now consider the trapped particle distribution function f_p^T. If the rotational transform per helical period is small, a line of force between the helical mirror points is localized in poloidal angle. Thus, $F_{p0}^{T.}$ depends on θ but not ζ, i.e.,

$$F_{p0}^{T.} = F_{p0}^{T.}(\varepsilon,\mu,r,\theta,t) \quad , \tag{13}$$

and unlike $F_{p0}^{U.T.}$, $F_{p0}^{T.}$ can have different values at different poloidal locations. Some stellarators, e.g., heliac, do not have small rotational transforms. Therefore, the line between the mirror points may have a finite poloidal excursion. However, including this effect in the transport calculation does not give a result which differs qualitatively from the result for the case when the line is localized in poloidal angle. Hence, for simplicity, any line between two mirror points is assumed to be fixed in poloidal angle in this study.

The expansion in $1/v_\parallel$ breaks down in a thin transition boundary layer of thickness $(\nu/\omega_b)^{1/2}$ between the trapped and untrapped regions in velocity space. This layer produces discontinuities in velocity-space flux between trapped and untrapped regions at all poloidal angles since particles leaving the trapped region at some θ can flow along B to a different θ before becoming essentially untrapped. Hence, only the total flux (i.e., the flux summed over θ) is continuous between trapped and untrapped regions [see Eq. (21)]. For a detailed treatment of the distribution function in the boundary layer using the Wiener-Hopf technique, see Hinton and Rosenbluth[21] and Shaing and Callen.[25]

Equation (5) to first order is

$$\frac{\partial F_{p0}}{\partial t} + \vec{v}_{\parallel}\cdot\vec{\nabla}F_{p1} + \vec{v}_D\cdot\vec{\nabla}F_{p0} + e\,\frac{\partial\Phi}{\partial t}\,\frac{\partial F_{p0}}{\partial\varepsilon} = C(F_{p0},F_0) \quad . \tag{14}$$

Solubility conditions on F_{p0} are obtained differently for untrapped particles than for the trapped particles. For untrapped particles, the above equation can be expressed as

$$\vec{B}\cdot\vec{\nabla}F_{p1}^{U.T.} = s \quad , \tag{15}$$

where

$$s \equiv -\frac{B}{v_{\parallel}}\left[\frac{\partial F_{p0}^{U.T.}}{\partial t} + \vec{v}_D\cdot\vec{\nabla}F_{p0}^{U.T.} + e\,\frac{\partial\Phi}{\partial t}\,\frac{\partial F_{p0}^{U.T.}}{\partial\varepsilon} - C(F_{p0}^{U.T.},F_0)\right] \quad .$$

Equation (15) is a "magnetic differential equation"[26]. Single-valued $F_{p1}^{U.T.}$ requires a solubility condition on $F_{p0}^{U.T.}$ obtained from the integration over the shell volume between two neighboring magnetic surfaces (constant pressure P surface) $p = P$ and $p = P + dP$, to vanish, i.e.,

$$\int_{shell} d\tau\,\frac{B}{v_{\parallel}}\left[\frac{\partial F_{p0}^{U.T.}}{\partial t} + \vec{v}_D\cdot\vec{\nabla}F_{p0}^{U.T.} + e\,\frac{\partial\Phi}{\partial t}\,\frac{\partial F_{p0}^{U.T.}}{\partial\varepsilon} - C(F_{p0}^{U.T.},F_0)\right] = 0 \quad . \tag{16}$$

Since $d\tau = -(dP/|\nabla P|)dS$ where dS is an area element on a magnetic surface, the solubility condition on $F_{P0}^{U.T.}$ can be expressed as

$$\int \frac{dS}{|\nabla P|}\,\frac{B}{v_{\parallel}}\left[\frac{\partial F_{p0}^{U.T.}}{\partial t} + e\,\frac{\partial\Phi}{\partial t}\,\frac{\partial F_{p0}^{U.T.}}{\partial\varepsilon} - C(F_{p0}^{U.T.},F_0)\right] = 0 \quad . \tag{17}$$

where we assume that the v_D term averages to zero.

For helically trapped particles, single valuedness of $F_{p1}^{T\cdot}$ requires the $\vec{v}_\parallel \cdot \vec{\nabla} F_{p1}^{T\cdot}$ term in Eq. (14) to vanish after applying the operator $\oint d\ell/v_\parallel$ between two mirror points. Defining a trapped particle bounce-average operator on any function G such that $\langle G \rangle \equiv (\oint d\ell/v_\parallel)^{-1} \oint d\ell G/v_\parallel$, and applying this operator to Eq. (14) gives the solubility condition on $F_{t0}^{T\cdot}$:

$$\frac{\partial F_{p0}^{T\cdot}}{\partial t} + \langle \vec{v}_D \rangle \cdot \vec{\nabla} F_{p0}^{T\cdot} + e \frac{\partial \Phi}{\partial t} \frac{\partial F_{p0}^{T\cdot}}{\partial \varepsilon} = \langle C(F_{p0}^{T\cdot}, F_0) \rangle \quad . \tag{18}$$

For helical wells localized in poloidal angle, the bounce-averaged drift velocity $\langle \vec{v}_D \rangle$ can be obtained in closed form if the parallel velocity is approximated by

$$v_\parallel \cong \pm \{\frac{2}{m} [\varepsilon - \mu B_0 (1 - \epsilon_h \cos(\ell\theta - m\zeta))]\}^{1/2} .$$

The result is[10]

$$\langle \vec{v}_D \rangle = v_B(\sin\theta \hat{e}_r + \cos\theta \hat{e}_\theta) + r(\Omega_E + \Omega_H)\hat{e}_\theta \quad , \tag{19}$$

where the expressions for v_B and Ω_E have already been given in Sec. III (v_B has a positive sign for electrons and a negative sign for ions), and

$$\Omega_H = \frac{v_B \ell \epsilon_h}{(r^2/R)} \left(\frac{2E(\kappa)}{K(\kappa)} - 1\right) \quad .$$

is the bounce-averaged poloidal rotational frequency. $K(\kappa)$ and $E(\kappa)$ are the elliptical integrals of the first and second kind, and their argument

$$\kappa \equiv \{(\frac{1}{2\mu B_0 \epsilon_h}) [\varepsilon - \mu B_0 (1 - \epsilon_h)]\}^{1/2} \quad ,$$

is essentially $v_{\parallel}/\sqrt{2\epsilon_h v_{\parallel}}$ at the local magnetic field minimum. For particles trapped at different depths in the helical well, the value of κ ranges from 0 to 1.

To conclude this section, the jump for the distribution function f_p across the boundary layer between the trapped and untrapped regions will now be established and evaluated.

Let $\xi = v_{\parallel}/v$ be the pitch-angle variable. Then, because of the small size of the boundary layer region in velocity space, $\Delta\xi$ is small, and f_p varies rapidly in pitch angle in this region. Thus, to the lowest order in small $\Delta\xi$, the dominant contribution to the Fokker-Planck collision operator in the boundary layer region is the pitch-angle scattering operator, i.e.,

$$\sum_j C_{pj}\,(f_p, f_j) \cong \frac{\sum_j \nu_{pj}}{4} \frac{\partial}{\partial\xi}\,(1-\xi^2)\,\frac{\partial f_p}{\partial\xi} \quad , \tag{20}$$

where $\nu = \langle\Delta v_{\perp}^2\rangle/v^2$ is the spitzer collision frequency [see Eq. (50)]. The condition for trapping is $|\xi|<|\xi_c| \cong (2\epsilon_h)^{1/2}$. The summation j is taken over all kinds of field particles (e.g., electrons, deuterons, and tritons). The reason that the coefficient is 1/4 instead of the usual 1/2 is because only the change in v^2 in the pitch-angle direction, rather than the change in the total v^2, is of concern to the trapping and detrapping processes.

Using the approximation (20), the boundary condition for the distribution function can be obtained by integrating the drift-Boltzmann equation [Eq. (5)] with respect to ξ across the boundary layer and then integrated over a thin shell between the two adjacent magnetic surfaces in order to eliminate the $\vec{v}_{\parallel}\cdot\vec{\nabla} f$ term. The result is[17]

$$\int_{\text{shell}} d\tau \, \frac{B}{v_\parallel} \frac{\partial f_p}{\partial \xi} \bigg|_{\xi_c^+} = \int_{\text{shell}} d\tau \, \frac{B}{v_\parallel} \frac{\partial f_p}{\partial \xi} \bigg|_{\xi_c^-} \quad . \tag{21}$$

Because f_p is continuous, we also have

$$\int_{\text{shell}} d\tau \, \frac{B}{v_\parallel} \ln[f_p^{U.T.}(\xi_c^+)] \frac{\partial f_p}{\partial \xi} \bigg|_{\xi_c^+} = \int_{\text{shell}} d\tau \, \frac{B}{v_\parallel} \ln[f_p^{T.}(\xi_c^-)] \frac{\partial f_p}{\partial \xi} \bigg|_{\xi_c^-} . \tag{22}$$

The continuity condition is

$$f_p^{U.T.}(\xi_c^+) = f_p^{T.}(\xi_c^-) \quad . \tag{23}$$

The reason for this condition is because, otherwise, there will be no other term in the drift-Boltzmann equation to balance the collision operator term, and the discontinuity will be smoothed out by collisions immediately.

B. Electron Transport

The electron step size is small compared to the minor radius. Thus

$$\frac{v_B}{a\nu_{eff}} \ll 1 \quad . \tag{24}$$

For example, using the reference stellarator parameters given in Table I, $v_B/a\nu_{eff} = \underline{O}(10^{-3})$ for thermal electrons. The radial ambipolar electric field can be obtained from the approximation $(e/T)(\partial\Phi/\partial r) \cong (1/n)(\partial n/\partial r)$. Then $\Omega_E = \underline{O}(10^3 \sec^{-1})$, and hence

$$\frac{\Omega_E}{\nu_{eff}} \ll 1 \quad . \tag{25}$$

Thus, for most cases, poloidal rotation is not important in the study of electron transport and thus we do not include it. A similar remark applies to

Ω_H. Note that inequalities (24) and (25) are also valid in some of the recent experimental stellarators with parameters given in Table I.

Inequality (24) suggests a perturbation analysis to solve Eqs. (17) and (18). Expanding F_{e0} in powers of $v_B/a\nu_{eff}$ gives

$$F_{e0} = f_{e0} + f_{e1} + f_{e2} + \cdots \quad . \tag{26}$$

The Ω_E and Ω_H terms will be treated as second order in this expansion. Since collisions are dominant [inequalities (24) and (25)] and Eqs. (16) and Eq. (18) result in no particle flow out of the magnetic surface in the lowest order in expansion Eq. (26), f_{e0} must be a Maxwellian by the Boltzmann H-theorem. This is formally proved by the following argument.

For untrapped electrons, Eq. (16) to lowest order is

$$\int_{\text{shell}} d\tau \, \frac{B}{v_\parallel} \sum_j C_{ej}(f_{e0}^{U.T.}, f_{j0}) = 0 \quad , \tag{27}$$

where the summation j is over electrons and ions. The ions are assumed to have no mean velocity but otherwise their distribution is arbitrary. Since $f_{e0}^{U.T.}$ is a function of only r, ε, and μ, the factor $\ln f_{e0}^{U.T.}$ can be inserted inside the integral in Eq. (27) so that

$$\int_{\text{shell}} d\tau \, \frac{B}{v_\parallel} \ln f_{e0}^{U.T.} \sum_j C_{ej}(f_{e0}^{U.T.}, f_{j0}) = 0 \quad . \tag{28}$$

For trapped electrons, Eq. (18) to lowest order is

$$\oint \frac{d\ell}{v_\parallel} \sum_j C_{ej}(f_{e0}^{T.}, f_{j0}) = 0 \quad . \tag{29}$$

Since $f_{e0}^{T.}$ is independent of ℓ, the factor $\ln f_{e0}^{T.}$ can be inserted inside the line integral and Eq. (29) becomes

$$\oint \frac{d\ell}{v_\parallel} \ln f^{T.}_{e0} \sum_j C_{ej}(f^{T.}_{e0}, f_{j0}) = 0 \quad . \tag{30}$$

Integrate Eqs. (28) and (30) with respect to ε and μ over the respective untrapped and trapped regions in phase space. Then convert the line integral condition for the trapped particles into a shell integral condition (see Ref. 17). Adding these two shell integrals for the untrapped and trapped electrons and then converting the combined integral into an ordinary velocity-space integral making use of the Jacobian relation

$$\int d^3v = \int \frac{4\pi B d\mu d\varepsilon}{m_e^2 |v_\parallel|} \quad ,$$

$$= \int \frac{4\sqrt{2}\pi}{m_e^{3/2}} d\xi \sqrt{\varepsilon + e\Phi}\, d\varepsilon \quad , \tag{31}$$

gives

$$\int_{\text{shell}} d\tau \int d^3v \ln f_{e0} \left[C_{ee}(f_{e0}, f_{e0}) + \sum_i C_{ei}(f_{e0}, f_{i0})\right] = 0 \quad . \tag{32}$$

The summation i is taken over the field ions. Note that f_{e0} satisfies boundary conditions given by Eqs. (21) and (23). Also note that, from Eq. (22), the boundary layer region does not give a contribution to Eq. (32).

Using the Boltzmann H-theorem and the argument given by Hinton and Hazeltine[27], Eq. (32) implies that f_{e0} must be Maxwellian (see Ref. 17). The Maxwellian must be independent of θ since $f^{U.T.}_{e0} = f_{eM}$ is. Hence

$$f_{e0} = f_{eM}$$

$$\equiv n_e \left(\frac{m_e}{2\pi T_e}\right)^{3/2} \exp\left(-\frac{\varepsilon + e\Phi}{T_e}\right) \quad , \tag{33}$$

where n_e, T_e, and Φ are functions of r and t. To this order, the dependence of n_e and T_e on r is arbitrary; this independence is determined by annihilation conditions in second order.

For untrapped electrons, the first-order equation is

$$\int_{\text{shell}} d\tau \, \frac{B}{v_\parallel} \sum_j C_{ej}(f_{e1}^{U.T.}) = 0 \quad , \tag{34}$$

where $C_{ej}(f_{e1})$ is the linearized collision operator. For trapped electrons, the first-order equation is

$$\langle \sum_j C_{ej}(f_{e1}^{T.}) \rangle = v_B \sin\theta \left.\frac{\partial f_{eM}}{\partial r}\right|_\varepsilon \quad . \tag{35}$$

In order to solve for $f_{e1}^{T.}$, let us write it as the sum of a homogeneous and an inhomogeneous solution of Eq. (35), i.e.,

$$f_{e1}^{T.} = \bar{f}_{e1} + \mathcal{F}_e(\xi)\sin\theta \quad , \tag{36}$$

with the boundary condition $\mathcal{F}_e(\xi_c) = 0$. Thus, Eq. (35) can be separated into two equations

$$\langle \sum_j C_{ej}(\mathcal{F}_e) \rangle = v_B \left.\frac{\partial f_{eM}}{\partial r}\right|_\varepsilon \quad , \tag{37a}$$

and

$$\langle \sum_j C_{ej}(\bar{f}_{e1}) \rangle = 0 \quad . \tag{37b}$$

Again using the H-theorem, it can be shown $f_{e1}^{T.}$ and $f_{e1}^{U.T.}$ are the perturbations of Maxwellians and therefore can be absorbed into the lowest-order solution.

Now consider $\mathcal{F}_e(\xi)$. If the size of the trapping region is small (i.e., $|\xi_c| \ll 1$), the dominant contribution to the Fokker-Planck collision operator in this region is the pitch-angle scattering operator. The bounce-averaged pitch-angle scattering operator is evaluated in Appendix A, and the result is

$$\langle \sum_j C_{ej}(\mathcal{F}_e) \rangle \cong \frac{(\nu_{ee}+\sum_i \nu_{ei})}{4} \frac{1}{J} \frac{\partial}{\partial \xi_0} JD \frac{\partial \mathcal{F}_e}{\partial \xi_0} \quad , \tag{38}$$

where

$$\xi_0 \equiv \left(\frac{\varepsilon-\mu B+e\Phi}{\varepsilon}\right)^{1/2} = \frac{v_\parallel}{v} \text{ at the center of a magnetic well.}$$

$$\kappa \equiv \frac{\xi_0}{(2\varepsilon_h)^{1/2}} \;,\; 0 < \kappa \le 1$$

and expressions for $D(\xi_0)$ and $J(\xi_0)$ are given in Appendix A. Substitution of Eq. (38) into the left-hand side of Eq. (37a) yields

$$\frac{(\nu_{ee}+\sum_i \nu_{ei})}{4} \frac{1}{J} \frac{\partial}{\partial \xi_0} JD \frac{\partial \mathcal{F}_e}{\partial \xi_0} = v_B \left.\frac{\partial f_{eM}}{\partial r}\right|_\varepsilon \quad . \tag{39}$$

The second boundary condition for $\mathcal{F}_e$ just outside the thin boundary layer must be established before solving for $\mathcal{F}_e$. Using the relation $d\xi_0/d\xi = \xi/\xi_0$ as indicated in Appendix A and assuming that the magnetic field is independent of the poloidal angle, Eq. (21) becomes

$$\oint d\theta \left(\frac{\partial \mathcal{F}_e}{\partial \xi_0} + \frac{\partial \bar{f}_{e1}}{\partial \xi_0}\right)\Bigg|_{\xi_0=\xi_c^-} = \oint d\theta \left.\frac{\partial f_{e1}^{U.T.}}{\partial \xi_0}\right|_{\xi_0=\xi_c^+} \quad .$$

Note that $\bar{f}_{e1} = f_{e1}^{U.T.} = 0$. Thus, the boundary conditions are

$$\oint d\theta \left.\frac{\partial \mathcal{F}_e}{\partial \xi_0}\right|_{\xi_0=\xi_c} = 0 \quad , \tag{40a}$$

and, from before,

$$\left.\mathcal{F}_e\right|_{\xi_0=\xi_c} = 0 \quad . \tag{40b}$$

Integrating Eq. (39) with respect to ξ_0 twice, using the above boundary conditions, and noting that $\partial\mathcal{F}_e/\partial\xi_0$ at $\xi_0 = 0$ is zero since $\mathcal{F}_e$ is even in ξ_0, we obtain

$$\mathcal{F}_e = -\frac{4}{(\nu_{ee}+\sum_i \nu_{ei})} v_B H(\xi_0,r) \left.\frac{\partial f_{eM}}{\partial r}\right|_{\varepsilon} \quad , \tag{41}$$

where

$$H(\xi_0,r) \equiv \int_{\xi_0}^{\xi_c} \int_0^{\xi_0'} \frac{J''}{J'D'} \, d\xi_0'' d\xi_0' \quad .$$

Here the primes indicate the arguments ξ_0' and ξ_0''. Note that $\xi_c \equiv (2\varepsilon_h)^{1/2}$ is in general a function of r. It can be shown (Ref. 17) that

$$H(\xi_0,r) = \varepsilon_h(r)(1-\kappa^2) \quad .$$

Equation (17) to second order is

$$\int \frac{dS}{|\nabla P|} \frac{B}{v_\parallel} \left(\frac{\partial f_{eM}}{\partial t} - e \frac{\partial \Phi}{\partial t} \frac{\partial f_{eM}}{\partial \varepsilon}\right) = \int \frac{dS}{|\nabla P|} \frac{B}{v_\parallel} \sum_j C_{ej}(f_{e2}^{U.T.}) \quad . \tag{42}$$

Equation (18) to second order is

$$\oint \frac{d\ell}{v_\parallel} [\frac{\partial f_{eM}}{\partial t} - e \frac{\partial \Phi}{\partial t} \frac{\partial f_{eM}}{\partial \varepsilon} + v_B \sin^2\theta \frac{\partial \mathcal{F}_e}{\partial r}$$

$$+ (v_B \cos\theta + r\, \Omega_E + r\, \Omega_H) \frac{\cos\theta}{r} \mathcal{F}_e]$$

$$= \oint \frac{d\ell}{v_\parallel} \sum_j C_{ej}(f^T_{e2}) \quad .$$

Equations (42) and (43) together represent an inhomogeneous symmetric integral equation for f_{e2}. The solubility conditions on the temporal evolution are that the inhomogeneous terms be orthogonal to 1 and v_2 (i.e., the particle and energy conservation properties of the collision operator). These two conditions yield constraints on f_{eM} and give the temporal evolution of its parameters n_e and T_e.

To determine the first solubility condition, we first integrate Eqs. (42) and (43) with respect to ε and μ over the respective untrapped and trapped regions. Then, the result for the trapped particles is summed over flux tubes to convert it into a shell integral. Finally, adding these two shell integrals gives

$$\int \frac{dS}{|\nabla P|} \int \frac{4\pi B d\mu d\varepsilon}{m_e^2 |v_\parallel|} [\frac{\partial f_{eM}}{\partial t} - e \frac{\partial \Phi}{\partial t} \frac{\partial f_{eM}}{\partial \varepsilon} + v_B \sin^2\theta \frac{\partial \mathcal{F}_e}{\partial r}$$

$$+ (v_B \cos\theta + r\, \Omega_E + r\, \Omega_H) \frac{\cos\theta}{r} \mathcal{F}_e] = 0 \quad . \tag{44}$$

It will now be shown that Eq. (44) is equivalent to the particle conservation law. To derive it to the lowest order approximation, we assume that the magnetic surfaces are concentric circles and ~~that~~ B is constant. Dividing

Eq. (44) by the total surface area of the torus, which is approximated by $(2\pi)^2 rR_0$, and noting that in the ξ, μ coordinates $\partial v_\parallel/\partial t = e(\partial\Phi/\partial t)(\partial v_\parallel/\partial\varepsilon)$, the first two terms on the left-hand side of Eq. (44) can be written as

$$\frac{1}{(2\pi)^2 rR_0} \int dS \int \frac{4\pi B d\mu d\varepsilon}{m_e^2|v_\parallel|} \left(\frac{\partial f_{eM}}{\partial t} - e\,\frac{\partial\Phi}{\partial t}\,\frac{\partial f_{eM}}{\partial\varepsilon}\right)$$

$$= \frac{\partial\langle n_e\rangle}{\partial t} \quad . \tag{45}$$

where $\langle n_e\rangle$ is the surface-averaged density. In evaluating the remaining terms on the left-hand side of Eq. (44), note that the Ω_E and Ω_H terms vanish after θ integration. The v_B terms can be combined and expressed as

$$\frac{1}{(2\pi)^2 rR_0} \int r d\theta R_0 d\zeta \int \frac{4\pi B d\mu d\varepsilon}{m_e^2|v_\parallel|}\, v_B \left(\sin^2\theta\, \frac{\partial \mathcal{F}_e}{\partial r} + \cos^2\theta\, \frac{\mathcal{F}_e}{r}\right)$$

$$= \frac{1}{r}\frac{\partial}{\partial r}\, r\, \frac{\pi}{(2\pi)^2 R_0} \int R_0 d\zeta \int d^3v\; v_B \mathcal{F}_e \quad ,$$

$$= \frac{1}{r}\frac{\partial}{\partial r}\, r\Gamma_e \quad , \tag{46}$$

which defines Γ_e, the electron particle flux per unit area. Substituting Eqs. (45) and (46) into Eq. (44) gives

$$\frac{\partial\langle n_e\rangle}{\partial t} + \frac{1}{r}\frac{\partial}{\partial r}\, r\Gamma_e = 0 \quad . \tag{47}$$

This is the particle conservation equation for electrons. To obtain the second solubility condition for the temporal evolution, Eqs. (42) and (43) are first multiplied by $m_e v^2/2$, and then a similar procedure to that employed in obtaining the particle conservation equation is used. The result is the energy conservation equation which has the form

$$\frac{\partial}{\partial t}\frac{3}{2}\langle n_e T_e\rangle + \frac{1}{r}\frac{\partial}{\partial r} rQ_e - e\Gamma_e \frac{\partial \Phi}{\partial r} = 0 \quad , \tag{48}$$

where $(3/2)\langle n_e T_e\rangle$ is the surface-averaged energy density, and the electron energy flux per unit area is

$$Q_e = \frac{\pi}{(2\pi)^2 R_0} \int R_0 d\zeta \int d^3v \frac{m_e v^2}{2} v_B \mathcal{F}_e \quad .$$

Note that Eq. (48) is obtained under the assumption that $T_e = T_i$, and depends on there being no mean parallel ion velocity; otherwise, additional terms will appear.[28]

The electron particle and energy fluxes will now be evaluated. Substituting Eq. (41) into the expression for the particle flux gives

$$\Gamma_e = -\frac{m\pi}{(2\pi)^2 R_0} \int_{-\pi/m}^{\pi/m} R_0 \, d\zeta \, \frac{4\sqrt{2}\pi}{m_e^{3/2}} \int_{-e\phi}^{\infty} d\varepsilon \sqrt{\varepsilon + e\phi}$$

$$\times \frac{4v_B^2}{(\nu_{ee} + \sum_i \nu_{ei})} \left[\int_0^{\xi_c(r)} H(\xi_0, r) d\xi\right] \left.\frac{\partial f_{eM}}{\partial r}\right|_\varepsilon \quad ,$$

where the ζ integration is over one helical period and $\xi_c(r)$ is the value of ξ for which $\xi_0 = \xi_c(r)$. Note that the integral

$$\int_{-\pi/m}^{\pi/m} R d\zeta \int_0^{\xi_c(r)} H d\xi = \frac{1}{2}\int_0^{\xi_c(r)} \mathcal{J} H d\xi_0 \quad ,$$

since

$$J = 2\int_{-\pi/m}^{\pi/m} R d\zeta \frac{d\xi}{d\xi_0}$$

(see Appendix A) and the function $H(\zeta_0,r)$ is non-zero only between $0 \leq \xi_0 \leq \xi_c$. It can be shown[17] that

$$\int_0^{\xi_c(r)} JHd\xi_0 = \frac{8}{9} \frac{[2\varepsilon_h(r)]^{3/2}R}{m} \quad .$$

Therefore, the electron particle flux per unit area can now be expressed as

$$\Gamma_e = -\frac{8}{9\pi}[2\varepsilon_h(r)]^{3/2} \frac{4\sqrt{2}\pi}{m_e^{3/2}} \int_{-e\Phi}^{\infty} d\varepsilon\sqrt{\varepsilon + e\Phi}\, \frac{v_B^2}{(\nu_{ee} + \sum_i \nu_{ei})} \left.\frac{\partial f_{eM}}{\partial r}\right|_\varepsilon \quad . \qquad (49)$$

From this equation, the electron diffusion coefficient at a given energy is found to be proportional to $[v_B^2/(\nu_{ee} + \sum_i \nu_{ei})][\varepsilon_h(r)]^{3/2}$. Thus, the rigorous calculation verifies the result of the heuristic argument.

To carry out the energy integration in Eq. (49), note that the reciprocal of the Spitzer[90] "deflection time" for electrons scattered by background electrons and ions in the asymptotic limit [$v \gg v_i$ since $(m_i/m_e)^{1/2} \gg 1$] is

$$\nu_{ee}(v) + \sum_i \nu_{ei}(v) = A_D \ell_e^3 \frac{[\Phi(\sqrt{X}) - G(\sqrt{X}) + 1]}{X^{3/2}} \qquad (50)$$

Here,

$$A_D \equiv \frac{8\pi e^4 Z^2 Z_i^2 n_i \ln\Lambda}{m_e^2} \quad ,$$

with the subscript j denoting the quantity for the field particles,

$$\ell_e \equiv \left(\frac{m_e}{2T_e}\right)^{1/2} ,$$

the Chandrasekhar function G is

$$G(\sqrt{x}) \equiv \frac{\Phi(\sqrt{x}) - \sqrt{x}\,\Phi'(\sqrt{x})}{2x} ,$$

$\Phi(\sqrt{x})$ is the usual error function, and

$$x \equiv \frac{\varepsilon + e\Phi}{T} .$$

Using this expression, Eq. (49) can be written as

$$\Gamma_e = -\frac{8}{9\pi}\left(\frac{cT}{eB_0R_0}\right)^2 \frac{[2\varepsilon_h(r)]^{3/2}}{A_D\ell_e^3}\, n_e \left\{ \int_0^\infty dx\sqrt{x}\, \frac{x^{3.5}e^{-x}}{[\Phi(\sqrt{x}) - G(\sqrt{x}) + 1]} \right.$$

$$\left. \times \left[\frac{1}{n_e}\frac{\partial n_e}{\partial r} - \frac{e}{T}\frac{\partial\Phi}{\partial r} + \left(x - \frac{3}{2}\right)\frac{1}{T}\frac{\partial T}{\partial r}\right]\right\} \div \int_0^\infty dx\sqrt{x}\, e^{-x} . \tag{51}$$

The electron energy flux per unit area can be obtained in an entirely analogous manner and is

$$Q_e = -\frac{8}{9\pi}\left(\frac{cT}{eB_0R_0}\right)^2 \frac{[2\varepsilon_h(r)]^{3/2}}{A_D\ell_e^3}\, n_eT \left\{ \int_0^\infty dx\sqrt{x}\, \frac{x^{4.5}e^{-x}}{[\Phi(\sqrt{x}) - G(\sqrt{x}) + 1]} \right.$$

$$\left. \times \left[\frac{1}{n_e}\frac{\partial n_e}{\partial r} - \frac{e}{T}\frac{\partial\Phi}{\partial r} + \left(x - \frac{3}{2}\right)\frac{1}{T}\frac{\partial T}{\partial r}\right]\right\} \div \int_0^\infty dx\sqrt{x}\, e^{-x} . \tag{52}$$

To exhibit the contribution to particle and energy diffusion of electrons with energy between ε and $\varepsilon + d\varepsilon$ (these contributions are equal to $d\Gamma_e/d\varepsilon$ and and $dQ_e/d\varepsilon$, respectively), the integrands in Eqs. (51) and (52) are plotted versus energy. Assuming $(1/n)(\partial n/\partial r) = (e/T)(\partial\Phi/\partial r) = (1/T)(\partial T/\partial r)$, the integrands become $[x^4 e^{-x}/(\Phi(\sqrt{x})-G(\sqrt{x})+1)](x+1/2)$ and $[x^5 e^{-x}/(\Phi(\sqrt{x})-G(\sqrt{x})+1)]$ $x(x+1/2)$ which are plotted versus x in Figs. 5(a) and 5(b), respectively. The figures show that electrons with approximately five and six times the thermal energy give the dominant contributions to particle and energy diffusion, respectively.

After integration, Eqs. (51) and (52) becomes

$$\Gamma_e = -\frac{8}{9\pi}\left(\frac{cT}{eB_0R_0}\right)^2 \frac{[2\varepsilon_h(r)]^{3/2}}{A_D\ell_e^3} n_e \left[14.4\left(\frac{1}{n_e}\frac{\partial n_e}{\partial r} - \frac{e}{T}\frac{\partial\Phi}{\partial r} - \frac{3}{2}\frac{1}{T}\frac{\partial T}{\partial r}\right) + 71.2\,\frac{1}{T}\frac{\partial T}{\partial r}\right] \tag{53a}$$

$$Q_e = -\frac{8}{9\pi}\left(\frac{cT}{eB_0R_0}\right)^2 \frac{[2\varepsilon_h(r)]^{3/2}}{A_D\ell_e^3} n_e T \left[71.2\left(\frac{1}{n_e}\frac{\partial n_e}{\partial r} - \frac{e}{T}\frac{\partial\Phi}{\partial r} - \frac{3}{2}\frac{1}{T}\frac{\partial T}{\partial r}\right) + 423.4\,\frac{1}{T}\frac{\partial T}{\partial r}\right] \tag{53b}$$

Substitution of the value of $A_D\ell_e^3$ into Eqs. (53a) and (53b) gives

$$\Gamma_e = -2(2\varepsilon_h(r))^{3/2}\frac{T_4^{7/2}}{B_4^2R_m^2}\left[14.4\left(\frac{1}{n_{14}}\frac{\partial n_{14}}{\partial r_m} - \frac{e}{T_4}\frac{\partial\Phi}{\partial r_m} - \frac{3}{2}\frac{1}{T_4}\frac{\partial T_4}{\partial r_m}\right) + 71.2\,\frac{1}{T_4}\frac{\partial T_4}{\partial r_m}\right] (10^{19}\ \mathrm{cm}^{-2}\cdot\mathrm{sec}^{-1}) \quad , \tag{54a}$$

$$Q_e = -2(2\epsilon_h(r))^{3/2} \frac{T_4^{9/2}}{B_4^2 R_m^2} [71.2 (\frac{1}{n_{14}} \frac{\partial n_{14}}{\partial r_m} - \frac{e}{T_4} \frac{\partial \Phi}{\partial r_m} - \frac{3}{2} \frac{1}{T_4} \frac{\partial T_4}{\partial r_m})$$

$$+ 423.4 \frac{1}{T_4} \frac{\partial T_4}{\partial r_m}] \; (10^{20} \; \mathrm{keV \cdot cm^{-2} \cdot sec^{-1}}) \quad , \tag{54b}$$

where r_m and R_m are in meters, B_4 is in units of 10 kG, n_{14} is in 10^{14} cm^{-3}, and T_4 and $e\Phi$ are in 10 keV. Equations (54a) and (54b) show that diffusion due to the temperature gradient (the thermal diffusion) is greater than that due to the combined contribution of density and electric potential gradients by factors of approximately three and four, respectively. These equations also show that Q_e/T is larger than Γ_e by a factor of approximately six. In Sec. V, the exact value of Φ is obtained by matching the electron and the ion particle fluxes. In Ref. 17, Eqs. (53a) and (53b) are be written in a form displaying Onsager symmetry.

C. Ion Transport

Ion transport is calculated in this section with the assumption that the helical well depth ϵ_h is constant across the minor radius. For most stellarators, however, ϵ_h increases with the minor radius. Thus, ions may be collisionlessly detrap out of and entrap into helical wells. As shown in Appendix B, for the reference stellarator, this effect is significant only for ions having energies somewhat more than three times the thermal energy. In the later part of the following section, it is shown that the dominant contribution to ion diffusion, without the effect of collisionless detrapping/entrapping, comes from ions with energies between three and four times the thermal energy. Thus, for nonconstant ϵ_h, inclusion of the effect of collisionless detrapping/entrapping will give an estimate of the ion flux which is less than the estimate obtained without this effect. [The reason is that the ion diffusion coefficient is proportional to ν for the case with the effect of collisionless detrapping and entrapping but proportional to $\nu^{1/2}$ for the case without this effect.] However, the estimate obtained in this section provides an upper bound for the ion flux.

Since the ion collision frequency is much lower than that of the electrons, the $\vec{E}_r x\vec{B}$ drift takes a trapped ion through several poloidal rotations during a collisional detrapping time. Using the reference stellarator parameters, it can be shown that

$$\frac{v_B}{a\nu_{eff}} \sim \frac{v_B}{a\Omega_E} = \underset{\sim}{O}(10^{-1}) \quad , \tag{55}$$

and Ω_E/ν_{ij} is large. The "rotational limit" mentioned in the rest of this paper refers to the case $\Omega_E/\nu_{ij} >> 1$. Equation (55) holds for ions with energies less than five times the thermal energy. Except for low energy ions, i.e., $\varepsilon < T$, Eq. (55) is valid for ions in all the machines with parameters given in Table I. Thus, Eqs. (17) and (18) can be solved by expanding F_{i0} in powers of $v_E/a\Omega_E$ or $v_B/a\Omega_E$:

$$f_{i0} = f_{i0} + f_{i1} + f_{i2} + \cdots \tag{56}$$

Since the ion collision time is much less than the plasma confinement time, f_{i0} is a Maxwellian. This is formally shown in Ref. 16 by Boltzmann H-theorem argument.

For untrapped ions, the first-order equation is

$$\int_{shell} d\tau \; \frac{B}{v_\parallel} \sum_j C_{ij} (f_{i1}^{U.T.}) = 0 \quad . \tag{57}$$

For trapped ions, it is

$$\langle \sum_j C_{ij} (f_{i1}^{T.}) \rangle = \Omega_E \frac{\partial f_{i1}^{T.}}{\partial \theta} + v_B \sin\theta \frac{\partial f_{iM}}{\partial r}\Big|_\varepsilon \quad . \tag{58}$$

In order to solve for $f_{i1}^{T.}$, again let

$$f_{i1}^{T.} = \bar{f}_{i1} + \mathcal{F}_i(\xi,\theta) \quad , \tag{59}$$

with $\mathcal{F}_i(\xi_c,\theta) = 0$ and $\bar{f}_{i1}$ a homogeneous solution. Similar to the electron case, $f_{i1}^{U.T.}$ and $\bar{f}_{i1}$ can be taken to be zero. Hence for a sinusoidally-shaped well, Eq. (58) has the form

$$\frac{\sum_j \nu_{ij}}{4J} \frac{\partial}{\partial \xi_0} JD \frac{\partial \mathcal{F}_i}{\partial \xi_0} = \Omega_E \frac{\partial \mathcal{F}_i}{\partial \theta} + v_B \sin\theta \frac{\partial f_{iM}}{\partial r}\Big|_\varepsilon \quad . \tag{60}$$

Recall from the heuristic argument that the dominant contribution to ion diffusion comes from the barely trapped ions, i.e., ions with $\kappa \sim 1$. As κ approaches unity, Eq. (60) can be simplified. Since $D \equiv (\kappa^2)^{-1} [E(\kappa)/K(\kappa) + (\kappa^2-1)]$ and thus,

$$\lim_{\kappa\to 1} D \cong \frac{1}{K(\kappa_P)} \quad . \tag{61}$$

Here κ_P is the location of the peak of the first-order distribution function near the trapped-untrapped boundary in phase space. Also note that

$$\lim_{\kappa\to 1} \{K(\kappa) - \frac{1}{2} \ln [16/(1-\kappa)]\} = 0 \quad . \tag{62}$$

Thus, near $\kappa=1$, the derivative $[\partial(JD)/\partial\xi_0](\partial\mathcal{F}_i/\partial\xi_0)$ is much smaller than $(JD)(\partial^2\mathcal{F}_i/\partial\xi_0{}^2)$ and Eq. (60) can be approximated by

$$\frac{\sum_j \nu_{ij}}{4K(\kappa_p)} \frac{\partial^2\mathcal{F}_i}{\partial\xi_0^2} = \Omega_E \frac{\partial\mathcal{F}_i}{\partial\theta} + v_B \sin\theta \left.\frac{\partial f_{iM}}{\partial r}\right|_\varepsilon \quad . \tag{63}$$

[Although Eq. (62) has a logarithmic singularity at $\kappa=1$, the value $1/K(\kappa_p)$ is finite since κ_p is not exactly equal to unity.]

As mentioned in the heuristic argument, the dominant contribution to diffusion is concentrated in a region of width $\underline{O}\,(\sqrt{\nu_i/\Omega_E})$ near $\kappa\sim1$ in phase space. Thus, the ξ_o variable can be transformed into a "boundary-layer" variable x, which is defined as,

$$x = \frac{\xi_0-\xi_c}{\epsilon_b} \, , \; -\infty < x \leq 0 \tag{64}$$

or

$$x\epsilon_b = (\kappa-1)\xi_c \quad , \tag{65}$$

where

$$\epsilon_b \equiv \left(\frac{\sum_j \nu_{ij}}{4K(\kappa_p)\Omega_E}\right)^{1/2} \ll 1 \quad .$$

Expressing Eq. (63) in terms of the varible x gives

$$\frac{\partial^2\mathcal{F}_i}{\partial x^2} = \frac{\partial\mathcal{F}_i}{\partial\theta} + \frac{v_B}{\Omega_E} \sin\theta \left.\frac{\partial f_{iM}}{\partial r}\right|_\varepsilon \quad . \tag{66}$$

Let

$$\mathcal{F}_i = A(x)\sin\theta + B(x)\cos\theta \quad , \tag{67}$$

with boundary conditions on $\mathcal{F}_i$ at $x = 0$ the same as the boundary conditions Eqs. (40a) and (40b). Then, it can be shown that in order to satisfy Eq. (66) and the boundary conditions, functions A(x) and B(x) must have the form:

$$A(x) = \frac{v_B}{\Omega_E} e^{x/\sqrt{2}} \sin \frac{x}{\sqrt{2}} \left.\frac{\partial f_{iM}}{\partial r}\right|_\varepsilon , \tag{68a}$$

$$B(x) = \frac{v_B}{\Omega_E} (1 - e^{x/\sqrt{2}} \cos \frac{x}{\sqrt{2}}) \left.\frac{\partial f_{iM}}{\partial r}\right|_\varepsilon . \tag{68b}$$

To study the behavior of F_i, the function A(x)sinθ and B(x)cosθ are plotted [in units normalized by $(v_B/\Omega_E)(\partial f_{iM}/\partial r)$] versus the normalized pitch angle variable $\kappa/\sqrt{2\varepsilon_h}$ in Fig. 6. Since the contribution of terms involving B(x) integrate to zero in the second order, we shall find that only the terms involving A(x) contribute to diffusion. Although the B(x) term does not contribute directly to diffusion, this term creates an non-radial ambipolar electric field which causes enhancement of electron and ion diffusion. This effect will be discussed in the following section. Figure 6 indicates that the function A(x) peaks near κ=1. This result confirms the heuristic argument.

The temporal evolution of the ion density and energy is obtained by going to second order in expansion (56). Using exactly the same procedure as in obtaining the electron particle flux, the contribution to the ion flux from ions with ϵ_b<<1 per unit area is

$$\Gamma_i = \frac{m\pi}{(2\pi)^2 R_0} \int_{-\pi/m}^{\pi/m} R_0 d\zeta \, \frac{4\sqrt{2}\pi}{m_i^{3/2}} \int_{\varepsilon_T}^{\infty} d\varepsilon \sqrt{\varepsilon - e\Phi} \, v_B \int_0^{\xi_c} d\xi \, A(x)$$

where ϵ_T is the "transition energy" below which the ordering given by Eq. (55) breaks down. Note that $J = 2\int_{-\pi/m}^{\pi/m} (d\xi/d\xi_0)\, R_0 d\zeta = (8\kappa K(\kappa)R)/m$ as indicated in Appendix A. Therefore, in the above equation

$$\int_{-\pi/m}^{\pi/m} R_0 d\zeta \int_0^{\xi_c(r)} A(x)d\xi = \frac{1}{2}\int_0^{\xi_c(r)} JA(x)d\xi_0 \quad ,$$

$$= \frac{1}{2}\epsilon_b \int_{-\infty}^{0} JA(x)dx \quad .$$

Substituting the expression for A(x) into this expression gives

$$\epsilon_b \int_{-\infty}^{0} JA(x)dx \cong -\frac{2}{\sqrt{2}}\frac{R}{m}\kappa_p\sqrt{K(\kappa_p)}\,\frac{v_B^2}{\Omega_E}\left(\frac{\sum_j \nu_{ij}}{\Omega_E}\right)^{1/2}\frac{\partial f_{iM}}{\partial r}\Bigg|_\epsilon \; .$$

Thus, the ion particle flux for $\epsilon>\epsilon_T$ is

$$\Gamma_i = \frac{1}{2\sqrt{2}}\left(\frac{\kappa_p\sqrt{K(\kappa_p)}}{\pi}\right)\frac{4\sqrt{2}\,\pi}{m_i^{3/2}}\int_{\epsilon_T}^{\infty} d\epsilon\sqrt{\epsilon-e\Phi}\,\frac{v_B^2}{\Omega_E}\left(\frac{\sum_j \nu_{ij}}{\Omega_E}\right)^{1/2}\frac{\partial f_{iM}}{\partial r}\Bigg|_\epsilon \quad . \tag{69}$$

The value of $\kappa_p\sqrt{K(\kappa_p)}$ can be evaluated by a iterative procedure. The value of κ to be used in the first step of the iteration is 0.8, which is the location of the peak of the $A(x)\sin\theta$ curve as shown in Fig. 6a. Then, from Eq. (62), $K(0.8) \approx 2.2$. The second step in the iteration is to use this value of K and Eq. (65) to obtain a new value of κ. Note that the value of A in Eq. (68a) peaks at $x = -\sqrt{2}\pi/4$. If $x = -\sqrt{2}\pi/4$, $\epsilon_b \approx 0.05$ (taken at $\epsilon = 4T$, the location of the peak of the curve as shown in Fig. 7), and $\xi_c = \sqrt{0.2}$, then Eq. (65) gives $\kappa \approx 0.87$. This scheme converges rapidly. After two more iterations, K converges to a value of 2.5 as κ_p approaches 0.88. The correction factor at $\kappa_p = 0.88$ is then

$$\frac{\kappa_p\sqrt{K(\kappa_p)}}{\pi} = 0.44 \quad . \tag{70}$$

As expected, this factor is less than unity (unity for rectangularly-shaped well is indicated in Ref. 16) since fewer particles can be trapped in a sinusoidally-shaped well than in a rectangularly-shaped well with length and depth equal to the length and the maximum depth of the sinusoidal well.

Equation (69) only gives the particle flux for ions with energies greater than ε_T. Low-energy trapped-ions cannot make a full poloidal rotation before they are detrapped by collision. Hence the low-energy ions are "non-rotational," i.e., $\Omega_E/\nu_{ij}\ll 1$ and then diffusive behavior is like that of the electrons. Consequently, the ion particle flux over the entire energy range can now be expressed approximately as

$$\Gamma_i = -\frac{8}{9\pi}\,(2\varepsilon_h(r))^{3/2}\,\frac{4\sqrt{2}\pi}{m_i^{3/2}}\int_{e\Phi}^{\varepsilon_T} d\varepsilon\sqrt{\varepsilon-e\Phi}\,\frac{v_B^2}{\sum\limits_j \nu_{ij}}\,\frac{\partial f_{iM}}{\partial r}\bigg|_\varepsilon$$

$$-\frac{0.44}{2\sqrt{2}}\,\frac{4\sqrt{2}\pi}{m_i^{3/2}}\int_{\varepsilon_T}^{\infty} d\varepsilon\sqrt{\varepsilon-e\Phi}\,\frac{v_B^2}{\Omega_E}\left(\frac{\sum\limits_i \nu_{ij}}{\Omega_E}\right)^{1/2}\frac{\partial f_{iM}}{\partial r}\bigg|_\varepsilon \quad . \tag{71a}$$

Similarly, the ion energy flux is

$$Q_i = -\frac{8}{9\pi}\,(2\varepsilon_h(r))^{3/2}\,\frac{4\sqrt{2}\pi}{m_i^{3/2}}\int_{e\Phi}^{\varepsilon_T} d\varepsilon\sqrt{\varepsilon-e\Phi}\,\left(\frac{m_i v^2}{2}\right)\frac{v_B^2}{\sum\limits_j \nu_{ij}}\,\frac{\partial f_{iM}}{\partial r}\bigg|_\varepsilon$$

$$-\frac{0.44}{2\sqrt{2}}\,\frac{4\sqrt{2}\pi}{m_i^{3/2}}\int_{\varepsilon_T}^{\infty} d\varepsilon\sqrt{\varepsilon-e\Phi}\,\left(\frac{m_i v^2}{2}\right)\frac{v_B^2}{\Omega_E}\left(\frac{\sum\limits_i \nu_{ij}}{\Omega_E}\right)^{1/2}\frac{\partial f_{iM}}{\partial r}\bigg|_\varepsilon \quad . \tag{71b}$$

Equations (71a) and (71b) apply to either deuteron or triton diffusion. Note that for the case of rectangularly-shaped magnetic well, the first-order trapped-ion distribution function can be solved exactly. This solution recovers, except the numerical coefficients, the first and second term on the right-hand side of Eq. (71) in the limit of $\Omega_E/\nu_i >> 1$ and $\Omega_E/\nu_i << 1$, respectively (see Ref. 16).

Equations (71a) and (71b) are, of course, only approximate. The transition energy ϵ_T is any energy such that for $\epsilon >> \epsilon_T$ solutions given by Eqs. (67) and (68) - the rotational solution - is valid while for $\epsilon << \epsilon_T$ the nonrotational electron-like solution is valid. For $\epsilon \approx \epsilon_T$ the full form of the collision integral must be kept. This has recently been done by Itoh et al.[29] and it has been found that a harmonic mean of the nonrotational and rotational results lead to a good approximation for the ion flux. The harmonic mean is the approximation employed by Kovrizhnykh[14,15]. A simpler approximation used here is to choose the value of ϵ_T at which the integrands (for $\epsilon > \epsilon_T$ and $\epsilon < \epsilon_T$) agree. Since $\epsilon_T/T << 1$ in most applications, under this condition the total flux can be approximated by the rotational solution.

The integrals in Eq. (71) will now be evaluated. Note that in the asymptotic limit ($\sqrt{m_i/m_e} >> 1$) the reciprocal of the 90° "deflection time" for deuterons scattered by field particles has the form

$$\sum_j \nu_{Dj}(v) = \nu_{DD}(v) + \nu_{DT}(v) \quad ,$$

$$= A_D \ell_D^3 \frac{\left[(\Phi(\sqrt{x}) - G(\sqrt{x})) + (\Phi(\sqrt{(m_T/m_D)x}) - G(\sqrt{(m_T/m_D)x})) \right]}{x^{3/2}} \quad ,$$

Here, A_D and ℓ_D are exactly the same as that for electrons except that m_e is replaced by the deuterium mass m_D. Thus, the deuteron particle flux is

$$\Gamma_D = -\frac{8}{9\pi}\left(\frac{cT}{eB_0R_0}\right)^2 \frac{(2\varepsilon_h(r))^{3/2}}{A_D\ell_D^3} n_D \left\{ \int_0^{x_T} dx\sqrt{x}\, \frac{x^{7/2}e^{-x}}{\sum_j(\Phi(\sqrt{x}j) - G(\sqrt{x}j))} \right.$$

$$\times \left[\frac{1}{n_D}\frac{\partial n_D}{\partial r} + \frac{e}{T}\frac{\partial\Phi}{\partial r} + \left(x - \frac{3}{2}\right)\frac{1}{T}\frac{\partial T}{\partial r}\right]$$

$$+ \frac{0.44}{2\sqrt{2}}\left[\left(\frac{cT}{eB_0R_0}\right)^2 /\Omega_E\right]\left(\frac{A_D\ell_D^3}{\Omega_E}\right)^{1/2} n_D \int_{x_T}^{\infty} dx\sqrt{x}\, x^{5/4} e^{-x}$$

$$\times \left[\sum_j(\Phi(\sqrt{x}j) - G(\sqrt{x}j))\right]^{1/2} \left.\left[\frac{1}{n_D}\frac{\partial n_D}{\partial r} + \frac{e}{T}\frac{\partial\Phi}{\partial r} + \left(x - \frac{3}{2}\right)\frac{1}{T}\frac{\partial T}{\partial r}\right]\right\}$$

$$\div \int_0^{\infty} dx\sqrt{x}\, e^{-x} \quad , \qquad (72)$$

and the deuteron energy flux is

$$Q_D = -\frac{8}{9\pi}\left(\frac{cT}{eB_0R_0}\right)^2 \frac{(2\varepsilon_h(r))^{3/2}}{A_D\ell_D^3} n_D T \left\{ \int_0^{x_T} dx\sqrt{x}\, \frac{x^{9/2}e^{-x}}{\sum_j(\Phi(\sqrt{x}j) - G(\sqrt{x}j))} \right.$$

$$\times \left[\frac{1}{n_D}\frac{\partial n_D}{\partial r} + \frac{e}{T}\frac{\partial\Phi}{\partial r} + \left(x - \frac{3}{2}\right)\frac{1}{T}\frac{\partial T}{\partial r}\right]$$

$$+ \frac{0.44}{2\sqrt{2}}\left[\left(\frac{cT}{eB_0R_0}\right)^2 /\Omega_E\right]\left(\frac{A_D\ell_D^3}{\Omega_E}\right)^{1/2} n_D T \int_{x_T}^{\infty} dx\sqrt{x}\, x^{9/4} e^{-x}$$

$$\times \left[\sum_j(\Phi(\sqrt{x}_j) - G(\sqrt{x}_j))\right]^{1/2} \left.\left[\frac{1}{n_D}\frac{\partial n_D}{\partial r} + \frac{e}{T}\frac{\partial\Phi}{\partial r} + \left(x - \frac{3}{2}\right)\frac{1}{T}\frac{\partial T}{\partial R}\right]\right\}$$

$$\div \int_0^{\infty} dx\sqrt{x}\, e^{-x} \quad . \qquad (73)$$

Here $x_T \equiv \varepsilon_T/T$. Note that x_T is generally less than unity; thus, ion fluxes can be well approximated by keeping only the second term (the rotational limit) on the right-hand side of Eqs. (72) and (73).

To display the contribution to particle and energy diffusion that is due to deuterons with energy between ε and $\varepsilon + d\varepsilon$, the integrands in the second term on the right-hand side of Eqs. (72) and (73) are plotted versus energy. Assuming $(1/n)(\partial n/\partial r) = (e/T)(\partial\Phi/\partial r) = (1/T)(\partial T/\partial r)$, the integrands become $x^{7/4}e^{-x}\,(\Phi(\sqrt{x}) - G(\sqrt{x}))^{1/2}\,(x - 3/2)$ and $x^{11/4}e^{-x}\,(\Phi(\sqrt{x}) - G(\sqrt{x}))^{1/2}(x - 3/2)$, respectively. These are plotted versus x in Fig. 7. The figure shows that deuterons with roughly three and a half times the thermal energy give the dominant contribution to particle diffusion while those with roughly four times the thermal energy give the dominant contribution to energy diffusion. These figures also indicate that at low energies, the ion diffusion is inward. The reason is that ion mobility in E_r reduces the ion flux.

After numerically integrating the second terms of Eqs. (72) and (73) from zero to infinity, we find the approximate deuteron particle and energy fluxes (assuming a 50% - 50% D-T plasma) are:

$$\Gamma_D \cong -\frac{0.44}{2\sqrt{2}}\left[\left(\frac{cT}{eB_0R_0}\right)^2/\Omega_E\right]\left(\frac{A_D\ell_D^3}{\Omega_E}\right)^{1/2} n_D\left[1.63\left(\frac{1}{n_D}\frac{\partial n_D}{\partial r} + \frac{e}{T}\frac{\partial\Phi}{\partial r} - \frac{3}{2}\frac{1}{T}\frac{\partial T}{\partial r}\right) + 4.63\,\frac{1}{T}\frac{\partial T}{\partial r}\right] \quad , \tag{74a}$$

$$Q_D \cong -\frac{0.44}{2\sqrt{2}}\left[\left(\frac{cT}{eB_0R_0}\right)^2/\Omega_E\right]\left(\frac{A_D\ell_D^3}{\Omega_E}\right)^{1/2} n_D T\left[4.63\left(\frac{1}{n_D}\frac{\partial n_D}{\partial r} + \frac{e}{T}\frac{\partial\Phi}{\partial r} - \frac{3}{2}\frac{1}{T}\frac{\partial T}{\partial r}\right) + 17.68\,\frac{1}{T}\frac{\partial T}{\partial r}\right] \quad . \tag{74b}$$

It can be shown that the triton fluxes are nearly equal to the deuteron fluxes. Thus, deuteron fluxes can be used to estimate the ion particle and energy confinement times. However, for steady-state reactor operation, the deuterium and tritium injection ratio may be different from n_D/n_T and proper adjustment needs to be made. From Eq. (74), the ion diffusion coefficient is $0.25\{[cT/(eBR)]^2/\Omega_E\}(A_D \ell_D^3/\Omega_E)^{1/2}$ which is smaller than that given in Ref. 10 by a factor of five. This discrepancy lies in the incorrect numerical integration over the proper energy weighting of the Maxwellian distribution function in Ref. 10.

Substitution of $A_D \ell_D^3$ into Eqs. (74a) and (74b) gives

$$\Gamma_D \cong -7.4 \left(\frac{r_m}{\partial\Phi/\partial r_m}\right)^{3/2} \frac{n_{14}^{3/2} T_4^{7/4}}{B_4^{1/2} R_m^2} \left[1.63 \left(\frac{1}{n_{14}} \frac{\partial n_{14}}{\partial r_m} + \frac{e}{T_4} \frac{\partial\Phi}{\partial r_m} - \frac{3}{2} \frac{1}{T_4} \frac{\partial T_4}{\partial r_m}\right) + 4.63 \frac{1}{T_4} \frac{\partial T_4}{\partial r_m}\right] (10^{19}\ \mathrm{cm}^{-2} \cdot \mathrm{sec}^{-1}) \quad , \tag{75a}$$

$$Q_D \cong -7.4 \left(\frac{r_m}{\partial\Phi/\partial r_m}\right)^{3/2} \frac{n_{14}^{3/2} T_4^{9/4}}{B_4^{1/2} R_m^2} \left[4.63 \left(\frac{1}{n_{14}} \frac{\partial n_{14}}{\partial r_m} + \frac{e}{T_4} \frac{\partial\Phi}{\partial r_m} - \frac{3}{2} \frac{1}{T_4} \frac{\partial T_4}{\partial r_m}\right) + 17.68 \frac{1}{T_4} \frac{\partial T_4}{\partial r_m}\right] (10^{20}\ \mathrm{keV} \cdot \mathrm{cm}^{-3} \cdot \mathrm{sec}^{-1}) . \tag{75b}$$

where n_{14} is the total ion density.

Finally, Eqs. (75a) and (75b) can be cast to a matrix form that possesses Onsager symmetry just as in the electron case. Also note that from Eqs. (75a) and (75b), the ratio of Q_D/T to Γ_D is roughly five and from Sec. IVB, the ratio of Q_e/T to Γ_e is roughly six. Since $\Gamma_e = \Gamma_i$, the ion energy confinement time should be comparable to the electron energy confinement time. This is confirmed by numerical example in Sec. V.

D. Enhanced Transport Induced by the Nonradial Electric Field Caused by Ion Drift

In the [redacted] rotational limit, the first-order trapped ion distribution function is essentially the cosθ dependent term over the bulk of the trapped region. This term has a maximum at $\theta = 0$ and a minimum at $\theta = \pi$. The reason for this behavior is that the poloidal $\hat{E}_r \times \hat{B}$ rotation and the shift of the drift orbits cause an excess of ions on the outer region and a deficiency of ions on the inner region of the torus. This first-order distribution function creates an imbalance of charge that gives rise to an ambipolar electric field E_p which has a θ component. This electric field has the effect of enhancing electron and ion diffusion. The effect on transport caused by this nonradial electric field was first considered by Mynick.[11] However, our approach and conclusions given in this section differ considerably from his. This section presents the calculation for the $\hat{E}_p \times \hat{B}$ drift induced by the nonradial ambipolar field. Then, the corrected first-order electron distribution function is obtained by including the $\hat{E}_p \times \hat{B}$ drift. Finally, using the corrected first-order distribution function, the enhanced particle and energy fluxes are obtained.

To obtain the ambipolar potential Φ_p induced by the perturbed ion density, the quasineutrality condition is applied. This condition requires that

$$\int d^3v\,(f_{iM} + f_i^1) = \int d^3v\, f_{eM} \quad . \tag{76}$$

Here $f_{iM} = n_i(r)\exp(-mv^2/2 - e\Phi_p/T)$ and $f_{eM} = n_e(r)\exp(-mv^2/2 + e\Phi_p/T)$, where Φ_p is the potential, necessary for charge neutrality, which produces E_p.

After expanding the factor $\exp(-e\phi_p/T)$ and using the quasineutrality approximation $n_e \cong n_i$, Eq. (76) becomes

$$\phi_p = \frac{T}{2en}\int d^3v\, f_i^1 \quad . \tag{77}$$

In the rotational limit $\Omega_E/\nu_{ij} \gg 1$, f_i^1 has the form

$$f_i^1 = \frac{v_B}{\Omega_E}\frac{\partial f_{iM}}{\partial r}\bigg|_\varepsilon \cos\theta \quad .$$

Thus,

$$\phi_p \cong \frac{T}{2en}\cos\theta \int_{\text{trapped}} d^3v\, \frac{v_B}{\Omega_E}\frac{\partial f_{iM}}{\partial r}\bigg|_\varepsilon \quad .$$

The component of the $\vec{E}_p \times \vec{B}$ drift normal to a magnetic surface is

$$\vec{v}_{E\times B}\cdot\hat{e}_r = -\frac{c\partial\phi_p}{rB\partial\theta}$$

$$= \frac{cT}{2reBn}\sin\theta \int_{\text{trapped}} d^3v\, \frac{v_B}{\Omega_E}\frac{\partial f_{iM}}{\partial r}\bigg|_\varepsilon \quad . \tag{78}$$

Note that $\Omega_E = (c/rB)(\partial\phi/\partial r)$. The ambipolar radial electric field $-\partial\phi/\partial r$ can be approximated by $C(T/e)(1/n)(\partial n/\partial r)$ where the coefficient C, of order unity, is determined in Sec. V by requiring the electron and ion particle fluxes to be ambipolar. Thus, Eq. (78) can be expressed as

$$\vec{v}_{E_p\times B}\cdot\vec{e}_r = -\frac{3}{4}\frac{cT}{eB_0R_0}\frac{(2\varepsilon_h(r))^{1/2}}{C(1/n)(\partial n/\partial r)}\sin\theta$$

$$\times\left(\frac{1}{n_i}\frac{\partial n_i}{\partial r} + \frac{e}{T}\frac{\partial\phi}{\partial r} + \frac{1}{T}\frac{\partial T}{\partial r}\right) \quad , \tag{79}$$

which is of $\underline{O}(cT\sqrt{2\varepsilon_h}/eBR)$. For $\varepsilon_h = 0.1$, $v_{E_p\times B}/v_B = 0.5$ at $\varepsilon = T$. The effect of this $\vec{E}_p \times \vec{B}$ drift on electron transport will be discussed now, and the effect on ion transport will be discussed later in this section.

Note that the radial component of $\vec{v}_{E_p\times B}$ and $\vec{v}_B$ are proportional to $\sin\theta$, and that their directions are parallel for electrons. Therefore, the modified electron diffusion coefficient is

$$D_e(\varepsilon) \sim \frac{1}{\nu}\left(\frac{cT}{eBR}\right)^2\left[\frac{\varepsilon}{T} + \sqrt{2\varepsilon_h}\right]^2 . \tag{80}$$

For example, if $\varepsilon_h = 0.1$, then the diffusion coefficient is enhanced by about 50% for thermal electrons. However, as we have found in Sec. IV B, electron particle and energy diffusion is dominated by particles having five or six times the thermal energy. Thus, when the proper energy weighing is considered, the electron particle and energy fluxes are only enhanced by about 20 and 15%, respectively. This is shown in the following calculation.

Since $\vec{v}_{E_p\times B}$ and $\vec{v}_B$ are the same order of magnitude, the first-order electron distribution, given by Eq. (41), must be modified. Including the $\vec{E}_p \times \vec{B}$ drift into Eq.(39) yields

$$\frac{(\nu_{ee} + \sum_i \nu_{ei})}{4}\frac{1}{J}\frac{\partial}{\partial\xi_0}JD\frac{\partial\mathcal{F}_e}{\partial\xi_0}$$

$$= \left[v_B\sin\theta + \frac{c}{B}\left(-\frac{\partial\Phi_p}{r\partial\theta}\right)\right]\left.\frac{\partial f_{eM}}{\partial r}\right|_\varepsilon . \tag{81}$$

Using the same procedure that was employed in solving Eq. (39), Eq. (81) gives

$$F_e = -\frac{4}{(\nu_{ee} + \sum_i \nu_{ei})}\left[v_B\sin\theta + \frac{c}{B}\left(-\frac{\partial\Phi_p}{r\partial\theta}\right)\right]H(\xi_0,r)\frac{\partial f_{eM}}{\partial r} . \tag{82}$$

Following Eq. (46), it can be shown that the modified electron particle flux per unit area is

$$\Gamma_e = \frac{m}{(2\pi)^2 R}\int_0^{2\pi} d\theta \int_{-\pi/m}^{\pi/m} R d\zeta \int d^3v\, [v_B \sin\theta + \frac{c}{B}(-\frac{\partial\phi}{r\partial\theta})]\, e$$

$$= -\frac{8}{9\pi}\left(\frac{cT}{eB_0R_0}\right)^2 \frac{\left(2\varepsilon_h(r)\right)^{3/2}}{A_D\ell^3} n_e \Big\{ \int_0^\infty dx\sqrt{x}\, \frac{x^{3.5}e^{-x}}{[(\Phi(\sqrt{x}) - G(\sqrt{x})) + 1]}$$

$$\times \Big[x - \frac{3}{4}\frac{\sqrt{2\varepsilon_h(r)}}{C(1/n_e)(\partial n_e/\partial r)}\left(\frac{1}{n_i}\frac{\partial n_i}{\partial r} + \frac{e}{T}\frac{\partial\phi}{\partial r} + \frac{1}{T}\frac{\partial T}{\partial r}\right)\Big]^2$$

$$\times \left(\frac{1}{n_e}\frac{\partial n_e}{\partial r} - \frac{e}{T}\frac{\partial\phi}{\partial r} + (x - \frac{3}{2})\frac{1}{T}\frac{\partial T}{\partial r}\right)\Big\}$$

$$+ \int_0^\infty dx\sqrt{x}\, e^{-x} \quad ,$$

$$= -\frac{8}{9\pi}\left(\frac{cT}{eB_0R_0}\right)^2 \frac{(2\varepsilon_h(r))^{3/2}}{A_D\ell^3} n_e$$

$$\times \Big\{\Big[14.4\left(\frac{1}{n_e}\frac{\partial n_e}{\partial r} - \frac{e}{T}\frac{\partial\phi}{\partial r} + \frac{3}{2}\frac{1}{T}\frac{\partial T}{\partial r}\right) + 71.2\,\frac{1}{T}\frac{\partial T}{\partial r}\Big]$$

$$- \frac{3}{2}\frac{\sqrt{2\varepsilon_h(r)}}{C(1/n_e)(\partial n_e/\partial r)}\left(\frac{1}{n_i}\frac{\partial n_i}{\partial r} + \frac{e}{T}\frac{\partial\phi}{\partial r} + \frac{1}{T}\frac{\partial T}{\partial r}\right)$$

$$\times \Big[3.8\left(\frac{1}{n_e}\frac{\partial n_e}{\partial r} - \frac{e}{T}\frac{\partial\phi}{\partial r} - \frac{3}{2}\frac{1}{T}\frac{\partial T}{\partial r}\right) + 14.4\,\frac{1}{T}\frac{\partial T}{\partial r}\Big]\Big\} \quad . \qquad (83)$$

The second term on the right-hand side in the last equation is the enhancement for the electron particle flux.

Similarly, the modified energy flux can be obtained and has the form

$$Q_e = -\frac{8}{9\pi}\left(\frac{cT}{eB_0R_0}\right)^2 \frac{(2\varepsilon_h(r))^{3/2}}{\lambda_D \ell^3} n_e T$$

$$\times \left\{ \left[71.2\left(\frac{1}{n_e}\frac{\partial n_e}{\partial r} - \frac{e}{T}\frac{\partial \phi}{\partial r} + \frac{3}{2}\frac{1}{T}\frac{\partial T}{\partial r}\right) + 423.4\,\frac{1}{T}\frac{\partial T}{\partial r}\right]\right.$$

$$-\frac{3}{2}\frac{\sqrt{2\varepsilon_h(r)}}{C(1/n_e)(\partial n_e/\partial r)}\left(\frac{1}{n}\frac{\partial n_i}{\partial r} + \frac{e}{T}\frac{\partial \phi}{\partial r} + \frac{1}{T}\frac{\partial T}{\partial r}\right)$$

$$\times \left.\left[14.4\left(\frac{1}{n_e}\frac{\partial n_e}{\partial r} - \frac{e}{T}\frac{\partial \phi}{\partial r} + \frac{3}{2}\frac{1}{T}\frac{\partial T}{\partial r}\right) + 71.2\,\frac{1}{T}\frac{\partial T}{\partial r}\right]\right\} \quad , \qquad (84)$$

where the $(3/2)[\sqrt{2\varepsilon_h}/C(1/n)(\partial n/\partial r)]$ term is the enhancement of the electron energy flux. The term involving $(v_{E_p \times B})^2$ has not been included in Eqs. (83) and (84) because this term would be smaller than any other term in these two equations. Equations (83) and (84) indicate that the enhanced electron particle transport due to the electric field caused by ion drift is about 20% of the ordinary electron particle transport, the corresponding factor is about 15% for energy transport. Equations (83) and (84) can be cast into a matrix that possesses Onsager symmetry.

The effect of the $\vec{E}_p \times \vec{B}$ drift on ion transport will now be discussed. Since the $\vec{E}_p \times \vec{B}$ and grad-B drifts are in opposite direction for ions, the modified diffusion coefficient for ions is

$$D_i(\varepsilon) \sim \frac{1}{\Omega_E}\left(\frac{cT}{eBR}\right)^2 \left(\frac{\varepsilon}{T} - \sqrt{2\varepsilon_h}\right)^2 \left(\frac{\nu_i}{\Omega_E}\right)^{1/2} \quad . \qquad (85)$$

Hence, it may be thought that the nonradial electric field reduces ion transport. However, this is not the case. In fact, the ion particle transport must be increased by the same amount as the enhanced electron loss in order to preserve charge neutrality. Since ion diffusion is very sensitive to the radial electric field, while electron diffusion is not (see Sec. V), a slight decrease in radial electric field increases the ion transport to restore the charge imbalance. The ion heat loss should be increased by a corresponding factor since both ion particle and energy losses are proportional to $\Omega^{-3/2}$.

The electron drift also creates a nonradial ambipolar electric field. However, the $\vec{E}_p \times \vec{B}$ drift caused by this nonradial electric field is smaller than the grad-B drift velocity by a factor of v_B/av_{eff}. Therefore, the corrections to the first-order electron and ion distribution functions are negligible, and this nonradial electric field has no important effect on random-walk type diffusion.

Throughout the rest of this paper, we will ignore the modification in transport produced by these nonradial fields.

V. RADIAL AMBIPOLAR ELECTRIC FIELD AND SCALING LAWS FOR CONFINEMENT

The expressions for the electron and ion particle fluxes given in Secs. IVB and IVC depend on the magnitude of the ambipolar electrostatic potential $\Phi(r)$. The first part of this section discusses the behavior of the electron and ion fluxes as the magnitude of the radial electric field $E_r = -\partial\Phi(r)/\partial r$ varies. The second part of this section presents a convenient method of determining the self-consistent radial ambipolar potential and discusses the scaling laws for confinement.

In this section, it is assumed for simplicity that the radial electric field is related to the density gradient by a constant C, i.e.,

$$\frac{e}{T}\frac{\partial\Phi}{\partial r} = -C\frac{1}{n}\frac{\partial n}{\partial r} \quad . \tag{86}$$

Using this condition, the electron and ion fluxes are plotted versus C (in Fig. 8) for two different central densities ~~in Fig. 8~~ for the reference stellarator at r=a/2. Note that the electron flux is independent of central density (see Sec. III).

In this plot, both the density and temperature profiles are assumed to be parabolic, i.e., $n(r) = n_0[1 - (r/a)^2]$ and $T(r) = T_0[1 - (r/a)^2]$. (The reason for choosing parabolic profiles is given later in this section.)

Figure 8 shows that the ambipolar condition $\Gamma_e = \Gamma_i$ is satisfied at $C = 0.7$ for a peak density $n_0 = 2 \times 10^{14}$ cm^{-3}. As n_0 decreases to 10^{14} cm^{-3}, the ambipolar condition is satisfied at three different values of C. This behavior of multiple roots for the ambipolar field has been discussed for stellarators by Mynick and Hitchon,[30] for tandem mirrors by Mirin et al.,[31] and for Elmo Bumpy Torus by Jaeger et al.[32] Of the three roots shown in Fig. 8, the one at C_2 is unstable. A slight decrease in the positive charge moves C_2 to the stable equilibrium C_3 with the direction of the radial electric field pointing toward the minor axis. On the other hand, a slight increase in the positive charge moves C_2 to the stable equilibrium C_1 with the radial electric field pointing away from the minor axis. Although the electron and ion particle fluxes are very small at the stable equilibrium C_1, as indicated in Fig. 8, the energy fluxes are not necessarily small. This is because the energy of the particles that gives the dominant contribution to energy diffusion is higher than the energy of the particles that gives the dominant contribution to particle diffusion. In the following calculations, the electric field that gives the stable equilibrium C_3 is taken. For low density operation, this electric field is likely to be the equilibrium field that the plasma will adjust to naturally, and for high density operation, this electric field is the only equilibrium field that can satisfy the ambipolar condition.

It is important to note that the ion flux is very sensitive to radial electric field variations near $C = 0$. The reason is that a small increase in the magnitude of the electric field causes the ions to execute full poloidal rotations. This drastically reduces the ion particle flux. In contrast, electrons are relatively insensitive to a change in radial electric field because the electron effective collision frequency is less than the $\hat{E}_r \times \hat{B}$ poloidal rotation frequency. Therefore, if a rough estimate of the magnitude of the ambipolar field is given (e.g., $\hat{E}_r = 0$), the electron particle diffusion is well approximated and should provide a good estimate for the total particle confinement time.

Once the behavior of particle fluxes as a function of the radial electric field is determined, the problem is reduced to the determination of the magnitude of this radial electric field. In principle, Fig. 8 can be used to obtain the magnitude of the self-consistent radial electric field. This method requires, however, a different set of curves for each set of machine parameters. To obviate this, we propose an approximate method which can be used for all machine parameters. The approximation is the same approximation that is used to obtain Eq. (71), i.e., below ε_T, the nonrotational limit for ion transport is employed and above ε_T, the rotational limit is employed. Thus, matching the two limits gives

$$\Omega_E = \left(\frac{0.44 \times 9\sqrt{\pi}}{16\sqrt{2}}\right)^{2/3} \frac{A_D \ell_D^3}{2\varepsilon_h(r)} \frac{\left[\Phi(\sqrt{\varepsilon_T/T}) - G(\sqrt{\varepsilon_T/T})\right]}{(\varepsilon_T/T)^{3/2}} \quad . \tag{87}$$

Since $\Omega_E = (c/rB)(\partial\Phi/\partial r) = -C(cT/reBn)(\partial n/\partial r)$, Eq. (87) can be rewritten as

$$|C| = M \frac{\left[\Phi(\sqrt{\varepsilon_T/T}) - G(\sqrt{\varepsilon_T/T})\right]}{(\varepsilon_T/T)^{3/2}} \quad , \tag{88}$$

and the machine dependent parameter is

$$M = 0.27 \times 10^{-2} \frac{a_m^2 B_4 n_{14}^2(r)}{\varepsilon_h(r) n_{014} T_4^{5/2}(r)} \quad . \tag{89}$$

Here, n_{014} is the central plasma density in 10^{14} cm^{-3}.

The second equation that related C to ε_T/T is obtained from the ambipolar condition $\Gamma_e = \Gamma_i$. This equation is derived in Ref. 17 and has the form

$$C = \frac{-D(\varepsilon_T/T)/2 + E(\varepsilon_T/T) - 0.93}{D(\varepsilon_T/T) + 0.21} , \tag{90}$$

where

$$D(\varepsilon_T/T) = \left(\frac{\varepsilon_T}{T}\right)^5 \int_0^1 dx \frac{x^4 \exp\left(-(\varepsilon_T/T)x\right)}{\left[\Phi\left(\sqrt{(\varepsilon_T/T)x}\right) - G\left(\sqrt{(\varepsilon_T/T)x}\right)\right]}$$
$$+ \frac{1}{\left[\Phi\left(\sqrt{\varepsilon_T/T}\right) - G\left(\sqrt{\varepsilon_T/T}\right)\right]^{3/2}} \left(\frac{\varepsilon_T}{T}\right)^5 \int_1^\infty dx \left[\Phi\left(\sqrt{(\varepsilon_T/T)x}\right)\right.$$
$$\left. - G\left(\sqrt{\varepsilon_T/T)x}\right)\right]^{1/2} x^{7/4} \exp\left(-(\varepsilon_T/T)x\right)$$

and

$$E(\varepsilon_T/T) = \left(\frac{\varepsilon_T}{T}\right)^6 \int_0^1 dx \frac{x^5 \exp\left(-(\varepsilon_T/T)x\right)}{\left[\Phi\left(\sqrt{(\varepsilon_T/T)x}\right) - G\left(\sqrt{(\varepsilon_T/x)T}\right)\right]}$$
$$+ \frac{1}{\left[\Phi\left(\sqrt{\varepsilon_T/T}\right) - G\left(\sqrt{\varepsilon_T/T}\right)\right]^{3/2}} \left(\frac{\varepsilon_T}{T}\right)^6 \int_1^\infty dx \left[\Phi\left(\sqrt{(\varepsilon_T/T)x}\right)\right.$$
$$\left. - G\left(\sqrt{(\varepsilon_T/T)x}\right)\right]^{1/2} x^{11/4} \exp\left(-(\varepsilon_T/T)x\right)$$

with $x = (\varepsilon/T)/(\varepsilon_T/T)$. Note that Eq. (90) involves only C and ε_T/T. With two equations for two unknowns, C and ε_T can be determined from Eqs. (88) and (90) if the machine parameters are given.

Equating the right-hand sides of Eqs. (88) and (90) gives

$$M = \left| \frac{\left(-D(\epsilon_T/T)/2 + E(\epsilon_T/T) - 0.93\right)(\epsilon_T/T)^{3/2}}{\left(\Phi(\sqrt{\epsilon_T/T}) - G(\sqrt{\epsilon_T/T})\right)\left(D(\epsilon_T/T) + 0.21\right)} \right| \quad . \tag{91}$$

The parameter M is plotted versus ϵ_T/T in Fig. 8(a) using Eq. (91). The parameter C is plotted versus ϵ_T/T in Fig. 7(b) using Eq. (90). For any given set of machine parameters, M can be determined from Eq. (89). Once M is known, ϵ_T/T can be found from Fig. 8(a) and then C from Fig. 8(b). Knowing the normalized strength of the ambipolar field C, the neoclassical particle and energy fluxes can then be determined. Figure 8(a) shows that when the value of M is sufficiently small (e.g., if density is low), the ambipolar condition can be satisfied at three values of C as mentioned in the beginning of this section.

The corresponding Eq. (88) for electrons can be obtained simply by multiplying the right-hand side of Eq. (88) by a factor of approximately 120. Then, it can be shown that $(\epsilon_T/T)_{electron} > 20$ for the reactor and the reference stellarator and $(\epsilon_T/T)_{electron} > 8$ for ATF and the small heliac. Thus, electron rotation has no important effect on transport.

The neoclassical fluxes are most easily specified by stating the confinement time τ, i.e., the time during which the particle and energy must be replaced to maintain a steady state. For a reactor, however, the evaluation of τ is complicated by the fact that the reactor will most likely operate near marginal stability set by some limiting modes (e.g., the ballooning instabilities). The profile of the critical pressure gradient for ballooning instabilities is obtained from MHD stability analysis. In some regions of the plasma, the plasma pressure gradient will be subcritical and the entire flux will be carried by neoclassical transport. In other regions, the plasma will be marginally unstable, i.e., the plasma pressure gradient exceeds the critical gradient by a small amount, and the flux will be carried partially by turbulent convection and partially by neoclassical transport (see Ref. 15 for a discussion on convective equilibrium and transport). Therefore, if the particle confinement time at any minor radius is approximated by

$$\tau_p = \frac{\int^r dr\ 2\pi r n_e(r)}{2\pi r \Gamma_e(r)} \quad , \tag{92}$$

where Γ_e is the neoclassical particle flux, then τ_p will be greater than or equal to the confinement time (because Γ_e is less than or equal to the actual flux). Thus, a reasonable estimate of the confinement time could be obtained by minimizing Eq. (92) with respect to minor radius. If n(r) and T(r) are parabolic, as assumed before (a good approximation if the plasma is marginally unstable over a good part of the radius),[18] then Eq. (92) has its minimum value near $r = a/2$. The same argument can be used to estimate the energy confinement time τ_ε. Hence, in quoting stellarator confinement times, the profiles are assumed to be parabolic and τ is evaluated at $r = a/2$. (For smaller experimental stellarators, this prescription should still give an adequate estimate of the effective confinement time.) Inserting the expression for Γ_e [given by Eq. (54a)] into Eq. (92) and subsequently simplifying the equation by using the parabolic profile assumption, Eq. (92) becomes

$$\tau_p = 0.16 \times 10^{-4} \left. \frac{n_{014}\ B_4^2\ R_m^2\ a_m^2}{(4.4 + C)\big(2\varepsilon_h(a/2)\big)^{3/2} T_{04}^{7/2}} \right| \quad , \tag{93}$$

where T_{04} is the central plasma temperature in 10 keV.

The energy confinement time is

$$\tau_\varepsilon = \frac{\int^r dr\ 2\pi r(3/2)n(r)T(r)}{2\pi r Q(r)} \quad , \tag{94}$$

where Q(r) is the neoclassical energy flux. Inserting Eq. (53b) into Eq. (94) gives the electron energy confinement time,

$$\tau_\varepsilon^e = 0.5 \times 10^{-5} \left.\frac{n_{014}\ B_4^2\ R_m^2\ a_m^2}{(5.4 + C)\left(2\varepsilon_h(a/2)\right)^{3/2} T_{04}^{7/2}}\right| \quad . \tag{95}$$

Using Eqs. (94), (95), and the equation for ion energy flux [Eq. (71b)], it can be shown that the ion energy confinement time is

$$\tau_\varepsilon^i \simeq R\,\tau_\varepsilon^e \quad , \tag{96}$$

where the ratio of the ion to electron energy confinement times is

$$R(\varepsilon_T/T) = \frac{5.4 + C}{\left[(-C - 0.5)E(\varepsilon_T/T) + F(\varepsilon_T/T)\right]} \tag{97}$$

with

$$F(\varepsilon_T/T) = \left(\frac{\varepsilon_T}{T}\right)^7 \int_0^1 dx \frac{x^6 \exp\left(-(\varepsilon_T/T)x\right)}{\left(\Phi(\sqrt{(\varepsilon_T/T)x}) - G(\sqrt{(\varepsilon_T/T)x}\right)}$$

$$+ \frac{1}{\left(\Phi(\sqrt{\varepsilon_T/T}) - G(\sqrt{\varepsilon_T/T})\right)^{3/2}} \left(\frac{\varepsilon_T}{T}\right)^7 \int_1^\infty dx \left[\left(\Phi\sqrt{(\varepsilon_T/T)x}\right) - G\left(\sqrt{(\varepsilon_T/T)x}\right)\right]^{1/2}$$

$$\times\ x^{15/4} \exp\left(-(\varepsilon_T/T)x\right) \quad .$$

The function R is plotted versus ε_T/T in Fig. 10. Note that, although the four sets of machine parameters listed in Table I are different, Eqs. (93)-(96) are still applicable since the expansion parameters used in obtaining the neoclassical fluxes are valid for all these machines, as mentioned in Secs. IVB and IVC.

Using Eqs. (93)-(96), the confinement times estimated for the four machines are given in Table II. The results show that in all the machines, the electron energy confinement time is comparable to the ion energy confinement time, but is only one third of the particle confinement time. Note that ϵ_T/T is less than unity for all cases. For the reactor, $n\bar{\tau}_\epsilon \approx 1.3 \times 10^{14}\ \mathrm{cm}^{-3}\cdot\mathrm{sec}$ [where $\bar{\tau}_\epsilon = (\tau_\epsilon^e + \tau_\epsilon^i)/2$] which roughly satisfies the Lawson criterion for ignition. Equation (96) shows that the parameters $n\bar{\tau}_\epsilon$ can be increased by increasing the major radious, the minor radius, the magnetic field, the plasma denstiy, or by decreasing the plasma temperature. Finally, Eqs. (95) and (96) show that for a fixed minor radius, $n\bar{\tau}_\epsilon$ is proportional to the aspect ratio squared or the volume squared. For fixed aspect ratio, $n\bar{\tau}_\epsilon$ is proportional to the aspect ratio squared or the volume squared. For fixed aspect ratio, $n\tau_\epsilon$ is proportional to $(\mathrm{volume})^{4/3}$. Thus, if cost scales with volume, it is cheaper to increase the aspect ratio than the overall dimensions.

VI. CONCLUSION

Stellarator neoclassical transport in the low-collisional regime is calculated by using the drift-Boltzmann equation. By expanding the drift-Boltzmann equation and then applying the solubility conditions, a set of reduced equations for trapped and untrapped particles is obtained in Sec. IV A. The electron distribution function satisfying the reduced equations is obtained in Sec. IV B by a second expansion. The electron fluxes are then calculated. It is found that the electron fluxes in most cases are relatively insensitive to variations in ambipolar electric field. Electrons with five to six times the thermal energy give the dominant contribution to electron diffusion. The ion fluxes are calculated in Sec. IV C. The radial electric- field is very efficient in reducing the ion fluxes. Thus, electron and ion particle fluxes are governed by electron diffusion. For a reactor plasma, the effect of collisionless detrapping/entrapping is important only at energies beyond the energy range (three to four times the thermal energy) that gives the dominant contribution to ion diffusion.

We have compared our results for electron diffusion to those of other authors'. Our results agree with those of Connor and Hastie[8] and with those of Kovrizhnykh in the nonrotational limit. However, those of Galeev and Sagdeev[10] are a factor of two smaller. This discrepancy can be traced to a factor of two error in their Eq. 2.40. The ion diffusion coefficient obtained in this paper is smaller than that given in Ref. 10 by a factor of five after the numercial integration for the energy weighting of the Maxwellian distribution function is carried out correctly. Diffusion due to temperature gradient is larger than that due to density and electric potential gradients for both electron and ion diffusion. The nonradial ambipolar electric field induced by ion drift enhances the particle transport by about 20% and energy transport by about 15%.

A convenient graphical method for determining the self-consistent radial ambipolar field and energy cofinement times for machines with different parameters but with parabolic density and temperature profiles is presented in Figs. 9 and 10. From the machine parameter M [Eq. (89)] one obtains ε_T/T from Fig. 9(a) and then one obtains the ambipolar field parameter C from Fig. 9(b). Then the electron confinement time τ_ε^e is given by Eq. (95) (which involves C) while Eq. (96) yields the ion confinement time τ_ε^i where R is obtained from Fig. 10. Note that only for very small values of ε_T/T is $\tau_\varepsilon^i \gg \tau_\varepsilon^e$. Numerical calculations show that electron energy confinement time is always comparable to that of the ions regardless of machine parameters. Although the neoclassical losses are large, it is shown that ignition can probably be achieved in a reasonable size reactor. Confinement scaling law shows that in order to increase $n\tau$, it is cheaper to increase the aspect ratio than the overall dimensions of the reactor.

ACKNOWLEDGMENTS

It is a pleasure to thank A. H. Boozer, J. L. Johnson, H. E. Mynick, E. R. Salberta, and S. Yoshikawa for constructive discussions. Work performed under the auspices of the U. S. Department of Energy by the Lawrence Livermore National Laboratory under contract number W-7405-ENG-48 and Princeton Plasma Physics Laboratory under contract number DE-AC02-76-CHO-3073.

Appendix A. BOUNCE AVERAGE OF THE PITCH-ANGLE SCATTERING OPERATOR

The bounce-average operator in Eq. (38) is

$$< \frac{\nu}{4} \frac{\partial}{\partial \xi}(1 - \xi^2) \frac{\partial f}{\partial \xi} > = \frac{(\nu/4)\oint(d\ell/v_\parallel)(\partial/\partial\xi)(1-\xi^2)(\partial f/\partial\xi)}{\oint (d\ell/v_\parallel)} \quad . \tag{A1}$$

Let the value of ξ at the center of a magnetic well be ξ_0. Using the first adiabatic invariant, it can be shown that at an arbitrary fixed position in a magnetic well

$$\frac{d\xi}{d\xi_0} = \frac{\xi_0}{\xi} \quad , \tag{A2}$$

where

$$\xi_0 \equiv \left(2\varepsilon_h\right)^{1/2}\kappa,$$

with $0 \le \kappa \le 1$. Using Eq. (A2) and the fact that $\xi_0^2 << 1$ for trapped particles, Eq. (A1) can be written as

$$<\frac{\nu}{4} \frac{\partial}{\partial \xi} (1 - \xi^2) \frac{\partial f}{\partial \xi}> \simeq \frac{(\nu/4)(\partial/\partial\xi_0)(\xi_0)^{-2} [\oint d\ell(\xi_0/\xi)(\oint d\ell\xi/\oint d\ell/\xi)(\partial f/\partial\xi_0)]}{\oint d\ell(\xi_0/\xi)} \quad . \tag{A3}$$

The integrals in the numerator and in the denominator are evaluated by keeping only the helical variations in the magnetic field strength [i.e., $B = B_0[(1 - \varepsilon_h)\cos(\ell\theta - m\zeta)]$. The results are:

$$\oint d\ell\ \xi = \oint d\ell[\varepsilon_h(\cos h\ell - \cos h\ell_{max})]^{1/2}$$

$$= \frac{4\sqrt{\epsilon_h}\,R}{m}\,[\sqrt{8}\;E(\kappa) + \sqrt{8}\;(\kappa^2 - 1)\;K(\kappa)] \quad ,$$

$$\oint \frac{d\ell}{\xi} = \oint \frac{d\ell}{[\epsilon_h(\cos h\ell - \cos h\ell_{max})]^{1/2}}$$

$$= \frac{4R}{\sqrt{\epsilon_h}\,m}\,[\sqrt{2}\;K(\kappa)] \quad ,$$

where $h\ell = \ell\theta - m\zeta$ and $K(\kappa)$ $[E(\kappa)]$ is the complete elliptical integral of the first [second] kind. The bounce-averaged pitch-angle scattering operator becomes

$$< \frac{\nu}{4}\frac{\partial}{\partial\xi}\,(1 - \xi^2)\,\frac{\partial f}{\partial\xi} > = \frac{\nu}{4}\,\frac{1}{J}\,\frac{\partial}{\partial\xi_0}\,JD\,\frac{\partial f}{\epsilon\xi_0} \quad , \tag{A4}$$

where

$$D \equiv (\kappa^2)^{-1}\left[\frac{E(\kappa)}{K(\kappa)} + (\kappa^2 - 1)\right] \quad ,$$

$$J \equiv \oint d\ell\,\frac{\xi_0}{\xi} = \frac{8\kappa K(\kappa)R}{m} \quad .$$

Appendix B HEURISTIC DERIVATION OF THE ION DIFFUSION COEFFICIENT WITH THE EFFECT OF COLLISIONLESS DETRAPPING AND ENTRAPPING

In stellarators with the depth of the helical wells dependent on the minor radius, ions can collisionlessly detrap or entrap from the helical well as shown in Fig. 11. This can be understood as follows. Superposition of the grad-B drift upon the poloidal $\hat{E}_r \times \hat{B}$ drift results in an outward shift of the center of the trapped-ion drift orbit. Consequently, the depth of the helical well changes with the poloidal location of a trapped ion. Hence, barely trapped ions can experience collisionless detrapping and entrapping.

If the helical well depth $\epsilon_h(r) = \delta_a(r/a)^{\ell}$ with δ_a a constant,[33] then helically trapped ions with pitch angle $\xi = \sqrt{2\delta_a}(r_c/a)^{\ell/2}$ can detrap at radius r_c. The change in helical well depth $\delta\epsilon_h(r)$ and the corresponding collisionless change in the trapping condition $\delta\xi_{CL}$ as r changes by an amount δr is

$$\frac{\delta\epsilon_h(r)}{h(r)} = \frac{2\delta\xi_{CL}}{\xi}$$

$$= \ell\frac{\delta r}{r} \quad . \tag{B1}$$

Since the shift of the center of the trapped ion drift orbit from the center of the magnetic surface is v_B/Ω_E, the fraction of ions, F, that can experience collisionless detrapping and entrapping is $\underline{O}[(\ell/2)\sqrt{2\delta_a}(v_B/a\Omega_E)]$.

Collisions also bring ions in and out of helical wells. In one poloidal rotation period, collisions change the pitch angle of the ions by an amount

$$\delta\xi_{coll} = \underline{O}\left(\frac{\nu_i}{\Omega_E}\right)^{1/2} \quad . \tag{B2}$$

Therefore, in order for the effect of collisionless detrapping and entrapping to play a significant role in ion transport, the collisionless change in the trapped condition $\delta\xi_{CL}$ due to the radial variation of the depth of the helical well should be greater than $\delta\xi_{coll}$, i.e.,

$$\delta\xi_{coll} < \delta\xi_{CL}$$

$$= \frac{\ell}{2}\frac{v_B}{a\Omega_E}\left[2\delta_a\left(\frac{r}{a}\right)^{\ell}\right]^{1/2} \quad . \tag{B3}$$

If $\delta_a = 0.3$, then for the reference stellarator, the condition for Eq. (B3) to hold is that ion energy $\varepsilon > 3T$, and for the stellarator reactor, the condition is that $\varepsilon > 4T$. The parameters for the reference stellarator and the stellarator reactor are given in Table I.

To estimate the diffusion coefficient, we need to evaluate the step size δr. Using Eqs. (B1) and (B2), it can be shown that

$$\frac{\delta r}{r} = \frac{2}{\ell\xi_c}\left(\frac{v_i}{\Omega_E}\right)^{1/2},$$

and hence,

$$\delta r = \frac{2a}{\ell\sqrt{2\delta}}\left(\frac{v_i}{\Omega_E}\right) \quad . \tag{B4}$$

The characteristic frequency $\overline{\nu}$ for a trapped ion to detrap is $\underline{O}(\Omega_E)$. Therefore, the diffusion coefficient is

$$D = \underline{O}(\delta r^2 \overline{\nu} F)$$

$$= \frac{v_B}{\Omega_E} \frac{a}{\sqrt{2\delta_a}} v_i \,, \tag{85}$$

for $\ell = 2$.

Note that the ion does not entrap in the lower region of the torus after collisionless detrapping from point A (see Fig. 12), because the rate of change in particle pitch angle due to collisions is slower than the rate of increase of the helical well strength as the particle drifts from an inner minor radius to an outer minor radius. Also note that even if the helical wells have poloidal symmetry, the probability for an ion to entrap at the poloidal location with poloidal angle θ, after detrapping at $-\theta$, is small due to pitch-angle scattering.

Kinetic calculations for the problem discussed in this appendix have been carried out be Mynick.[34] However, in Mynick's calculation, it is assumed that particles always entrap at θ after detrapping at $-\theta$. A correct treatment of this problem with pitch-angle scattering would be a good subject for investigation.

Even if ε_h is constant across the minor radius, it might still be thought that the magnetic field variation on the trapped ion drift orbit caused by the variation in the toroidal field strength would collisionlessly detrap and entrap ions. This is not generally the case because, if the helical well length is assumed to be independent of its poloidal location, then the effect is compensated by E_r. This can be seen from the following argument. As a trapped ion changes its radius by Δ, it changes its kinetic energy by an amount

$$\frac{m\delta v^2}{2} = e\Delta E_r \quad ,$$

$$= \frac{ev_B Br}{c} ,$$

$$= - \frac{mv_\perp^2}{2} \frac{r}{R_0} ,$$

in order to conserve total energy. But by the conservation of the first adiabatic invariant,

$$\delta\left(\frac{mv_\perp^2}{2}\right) = \frac{mv_\perp^2}{2} \frac{\delta B}{B} ,$$

$$= - \frac{mv_\perp^2}{2} \frac{r}{R_0} .$$

Thus, $v_\parallel^2$ is unchanged at corresponding points in the helical well. (This also follows from the conservation law for the second adiabatic invariant.) Now, for ϵ_h independent of r [as in helical-axis stellarators (Heliac)], the helical trapped-region in velocity space expands by an amount r/R_0 as one moves from the inner (smaller R) to the outer (larger R) region of the torus. At the same time, the ion perpendicular velocity is reduced by the same factor of r/R_0 as indicated above. As a result, the fraction of trapped ions remains constant and the toroidal magnetic field variation causes no detrapping or entrapping.

REFERENCES

1. J. L. Johnson, Nucl. Technol./Fusion, 4, 1275 (1983).
2. R. S. Pease, in Plasma Physics and Controlled Fusion Research, 1984 (IAEA, Vienna, 1985), Vol. 3, p. 457.
3. D. V. Bartlett, G. Cannici, G. Cattanei, D. Dorst, G. Grieger, H. H. Hacker, J. How, H. Jäckel, R. Jaenicke, P. Javel, J. Junker, M. Kick, R. Lathe, J. Meyer, C. Mahn, S. Marlier, G. Müller, W. Ohlendorf, F. Rau, H. Renner, H. Ringler, J. Sapper, P. Smeulders, M. Tutter, B. Ulrich, A. Weller, E. Würsching, H. Wobig, M. Zippe, D. Cooper, K. Freudenberger, G. Lister, W. Ott, E. Speth, et al. in Plasma Physics and Controlled Nuclear Fusion Research, 1980 (IAEA, Vienna, 1981), Vol. 1, p. 185.
4. A. Iiyoshi, M. Sato, O. Motojima, T. Mutoh, S. Sudo, M. Iima, S. Kinoshita, H. Kaneko, H. Zushi, S. Besshou, K. Kondo, and K. Uo, Phys. Rev. Lett. 48, 745 (1982).
5. A. H. Boozer, T. K. Chu, R. L. Dewar, H. P. Furth, J. A. Goree, J. L. Johnson, R. M. Kulsrud, D. A. Monticello, G. Kuo-Petravic, G. V. Sheffield, and S. Yoshikawa in Plasma Physics and Controlled Nuclear Fusion Research, 1982 (IAEA, Vienna, 1983), Vol. 3., p. 129.
6. V. D. Shafranov, Phys. Fluids 26, 357 (1983).
7. E. A. Frieman, Phys. Fluids 13, 490 (1970).
8. J. W. Connor and R. J. Hastie, Phys. Fluids 17, 114 (1974).
9. A. A. Galeev, R. Z. Sagdeev, H. P. Furth, and M. N. Rosenbluth, Phys. Rev. Lett. 22, 511 (1969).
10. A. A. Galeev and R. Z. Sagdeev, Review of Plasma Physics, edited by M. A. Leontovich (Consultants Bureau, New York, 1979), Vol. 7, p. 307.
11. H. E. Mynick, Phys. Fluids 27, 2086 (1984).

12. A. H. Boozer and G. Kuo-Petravic, Phys. Fluids 24, 851 46 (1981).

13. A. H. Boozer, private communication.

14. L. M. Kovrizhnykh, Nucl. Fusion 24, 851 (1984).

15. L. M. Kovrizhnykh, Nucl. Fusion 24, 435 (1984).

16. D. D.-M. Ho and R. M. Kulsrud, Princeton Plasma Physics Laboratory, PPPL-2252, 1985.

17. D. D.-M. Ho and R. M. Kulsrud, Princeton Plasma Physics Laboratory, PPPL-2253, 1985.

18. D. D.-M. Ho and R. M. Kulsrud, Princeton Plasma Physics Laboratory Report No. PPPL-2251, 1985 (to be published).

19. J. W. Connor, J. P. Taylor, and M. F. Turner, Nucl. Fusion 24, 642 (1984).

20. L. Spitzer, Physics of Fully Ionized Gases (Wiley, New York, 1962), p. 131.

21. P. H. Rutherford and E. A. Frieman, Phys. Fluids 11, 569 (1968).

22. J. B. Taylor and R. J. Hastie, Plasma Phys. 10, 479 (1968).

23. J. L. Johnson, private communication.

24. F. L. Hinton and M. N. Rosenbluth, Phys. Fluids 16, 836 (1973).

25. K. C. Shaing and J. D. Callen, Phys. Fluids 25, 1012 (1982).

26. M. D. Kruskal and R. M. Kulsrud, Phys. Fluids 1, 265 (1958).

27. F. L. Hinton and R. D. Hazeltine, Rev. Mod. Phys. 48, 239 (1976).

28. M. N. Rosenbluth, R. D. Hazeltine, and F. L. Hinton, Phys. Fluids 13, 116 (1972).

29. K. Itoh, S.-I. Itoh, and R. M. Kulsrud, J. of Phys. Soc. of Japan, in press.

30. H. E. Mynick, Nucl. Fusion 23, 1053 (1983).

31. A. A. Mirin, S. P. Auerback, R. H. Cohen, J. M. Gilmore, L. D. Pearlstein, M. E. Rensink, Nucl. Fusion 23, 703 (1983).

32. E. F. Jaeger, D. A. Spong, C. L. Hedrick, Phys. Rev. Lett. 44, 866 (1978).

33. A. I. Morozov and L. S. Solovev, Review of Plasma Physics, edited by M. A. Leontovich (Consultants Burea, New York, 1966), Vol. 2, P. 1.

34. H. E. Mynick, Phys. Fluids 26, 2609 (1983).

TABLE I. STELLARATOR PARAMETERS

Physical quantity	Reactor	Reference stellarator	ATF[a]	Small[b] Heliac
Peak plasma density (cm^{-3})	7×10^{14}	2×10^{14}	10^{14}	10^{14}
Peak plasma temperature (keV)	10	10	1	1
Toroidal magnetic field (kG)	60	50	18	10
Peak β	15.6	6.4	2.5	8
R(m)	10	10	2.1	1.2
a(m)	1.0	1.0	0.3	0.25
$\varepsilon_h(r=a/2)$	0.1	0.1	0.2	0.1
Deuteron thermal velocity ($cm \cdot sec^{-1}$)	1.1×10^8	1.1×10^8	3.4×10^7	3.4×10^7
Deuteron 90° deflection time (sec)	2.3×10^{-3}	7.0×10^{-3}	0.44×10^{-3}	0.44×10^{-3}

[a] Reference 13.
[b] Reference 23.

TABLE II. Confinement Properties in Stellarators[a]

Confinement Parameters	Reactor	Reference Stellarator	ATF	Small Heliac
Particle confinement time τ_p(sec)	0.78	0.18	0.133	0.010
Electron energy confinement time τ_ε^e(sec)	0.21	0.05	0.036	0.003
Ion energy confinement time τ_ε^i(sec)	0.17	0.07	0.040	0.003
R	0.83	1.3	1.2	1.25
M	1.31	0.30	0.69	0.60
C	1.4	0.5	0.9	0.8
ε_T/T	0.63	0.38	0.47	0.44

[a] In this table, all results are obtained with parabolic density and temperature profiles at $r = a/2$.

FIGURE CAPTIONS

Fig. 1 Toroidal coordinate system (r, θ, ζ).

Fig. 2 The variation in B, the magnitude of the magnetic field, along a field line.

Fig. 3 Trapped and untrapped regions in velocity space, in terms of the parallel $(v_{\parallel})$ and perpendicular $(v_{\perp})$ velocity. The trapped region is shaded. The pitch angle θ of the gyro-orbit is defined by $\cos\theta = v_{\parallel}/v$.

Fig. 4 Projection of a typical collisionless ion orbit on a poloidal cross section. Point O is the center of the magnetic surface and $\Delta \equiv v_B/\Omega_E$.

Fig. 5 The relative electron fluxes per unit energy as a function of normalized energy $x = \varepsilon/T$.

(a). The relative electron particle flux per unit energy, $[x^4 e^{-x}/(\Phi(\sqrt{x}) - G(\sqrt{x}) + 1)](x + 1/2)$, as a function of x.

(b). The relative electron energy flux per unit energy, $[x^5 e^{-x}/(\Phi(\sqrt{x}) - G(\sqrt{x}) + 1)](x + 1/2)$, as a function of x.

Fig. 6 A and B as a function of pitch-angle parameter κ for ion energy at $\varepsilon = 4T$.

Fig. 7 The relative ion fluxes per unit energy as a function of normalized energy $x = \varepsilon/T$.

(a). The relative ion particle flux per unit energy, $x^{7/4} e^{-x}(\Phi(\sqrt{x}) - G(\sqrt{x}))^{1/2}(x - 3/2)$, as a function of x.

(b). The relative ion particle flux per unit energy, $x^{11/4} e^{-x}(\Phi(\sqrt{x}) - G(\sqrt{x}))^{1/2}(x - 3/2)$, as a function of x.

Fig. 8 Plot of the electron and ion particle fluxes Γ versus the normalized ambipolar electric field strength C for the reference stellarator at $r/a = 0.5$.

Fig. 9 Diagrams for the determination of ambipolar electric field.

(a). Plot of the machine dependent parameter M [given by Eq. (91)] versus ϵ_T/T.

(b). Plot of the normalized ambipolar electric field C [given by Eq. (90) versus ϵ_T/T.

Fig. 10 Plot of the ratio of the ion energy to electron energy confinement time, R [given by Eq. (97)], versus ϵ_T/T.

Fig. 11 Projection of a typical collisionless ion orbit on a poloidal cross section with the effect of collisionless detrapping and entrapping. Point A is the collisionless entrapping point where toroidally trapped ions enter the helical well. Point B is the collisionless detrapping point where ions leave the helical well and become toroidally trapped particles. Point O is the center of the magnetic surface and $\Delta \equiv v_B/\Omega_E$.

#85T0118

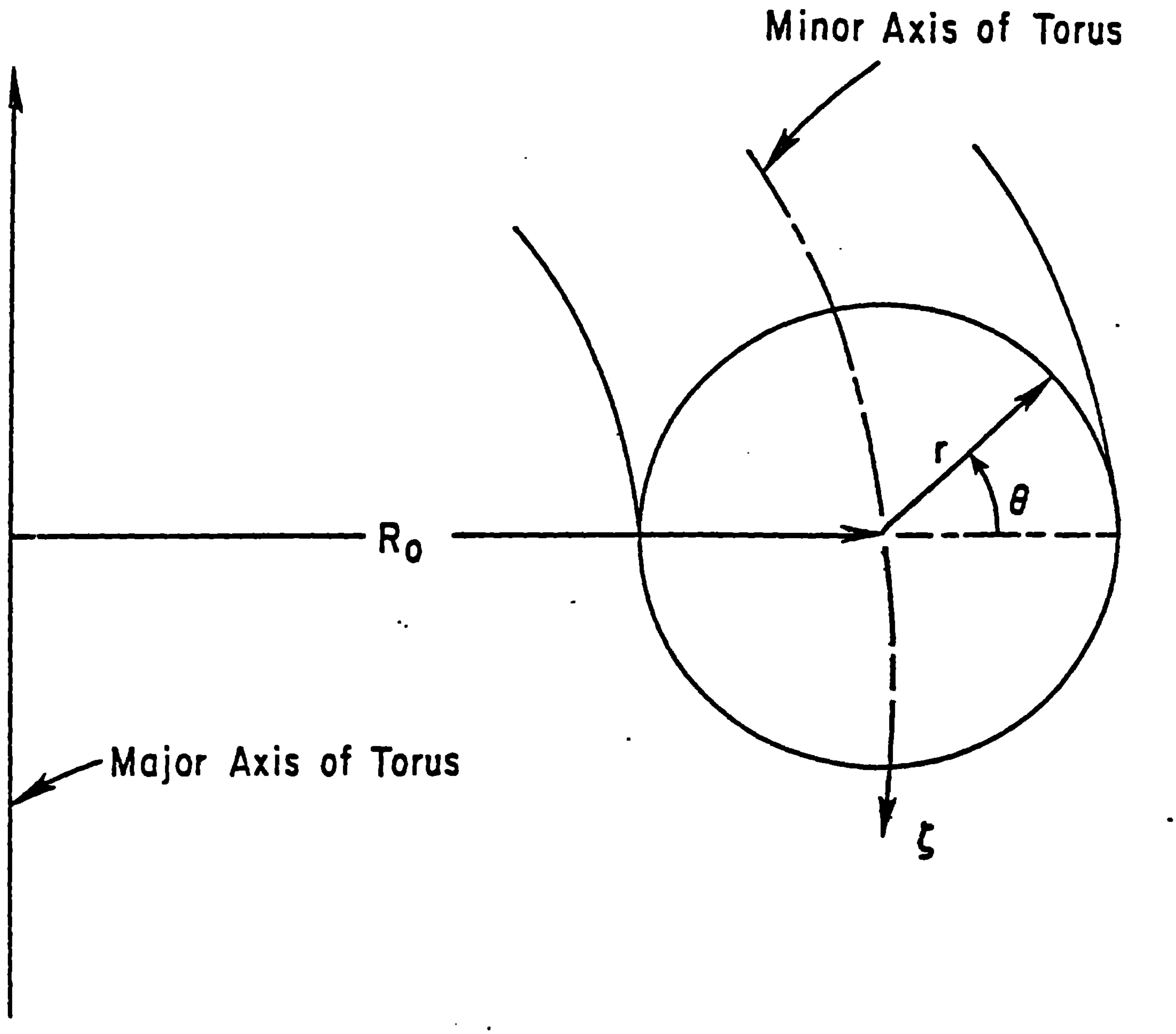

Fig. 1

#85T0200

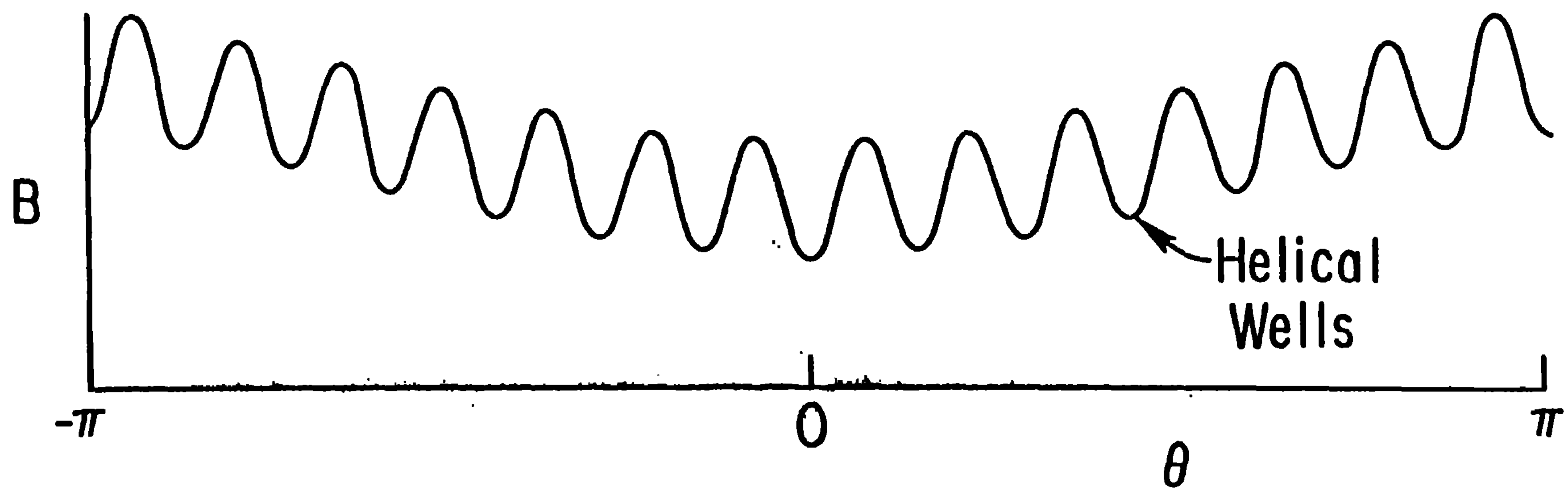

Fig. 2

#85T0117

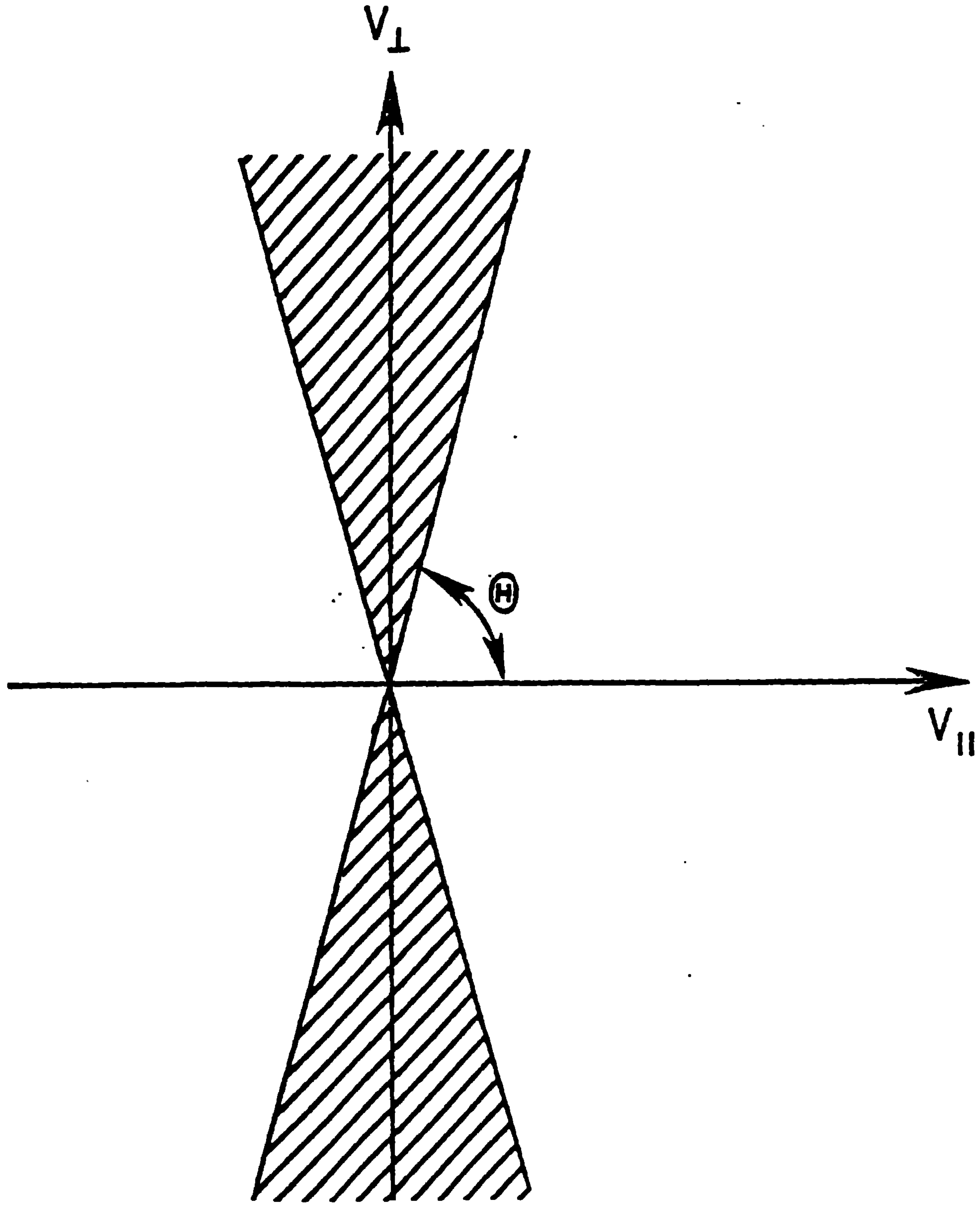

Fig. 3

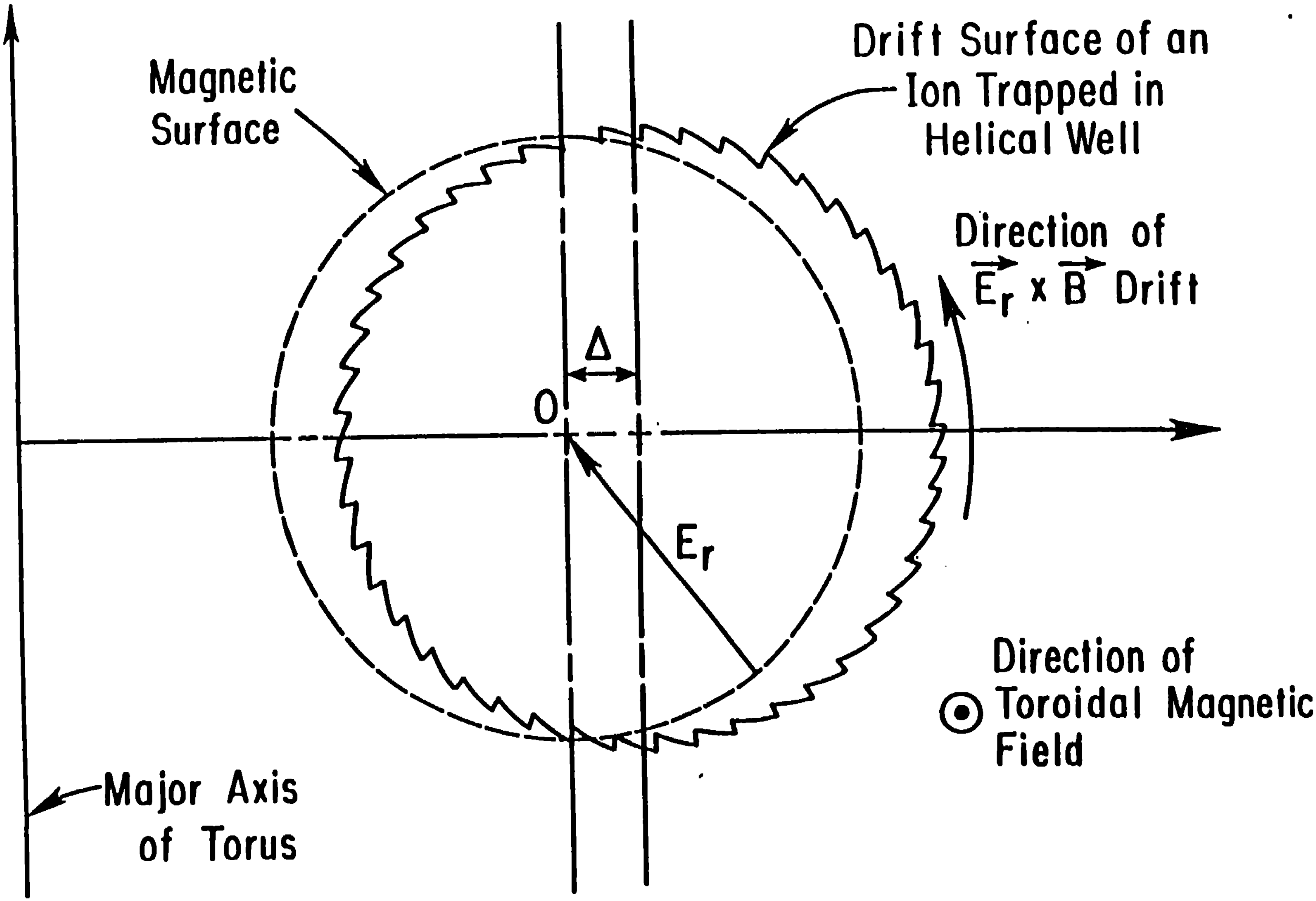
Magnetic Surface
Drift Surface of an Ion Trapped in Helical Well
Direction of $\vec{E}_r \times \vec{B}$ Drift
Δ
O
E_r
Direction of Toroidal Magnetic Field
Major Axis of Torus

Fig. 4

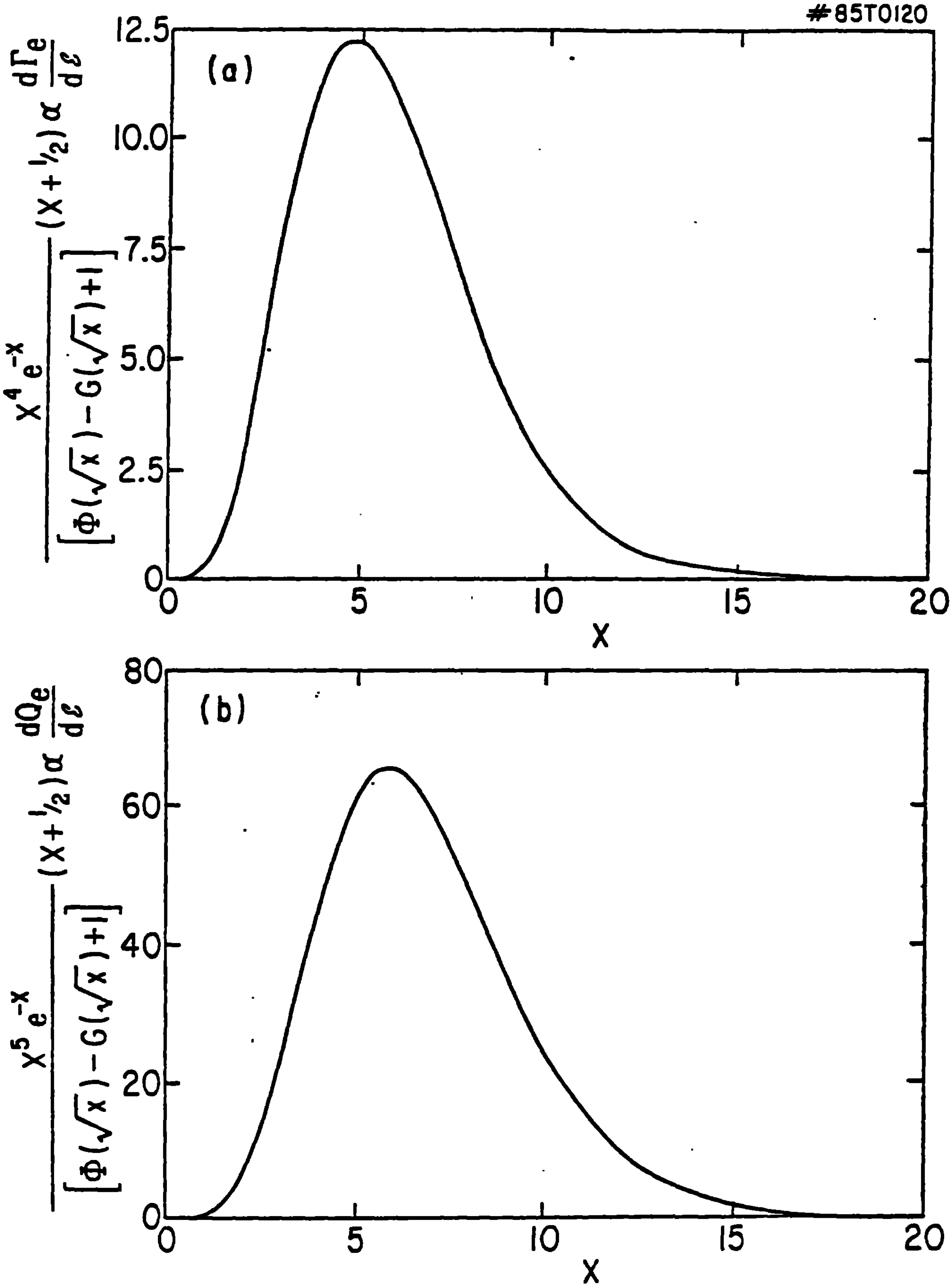

Fig. 5

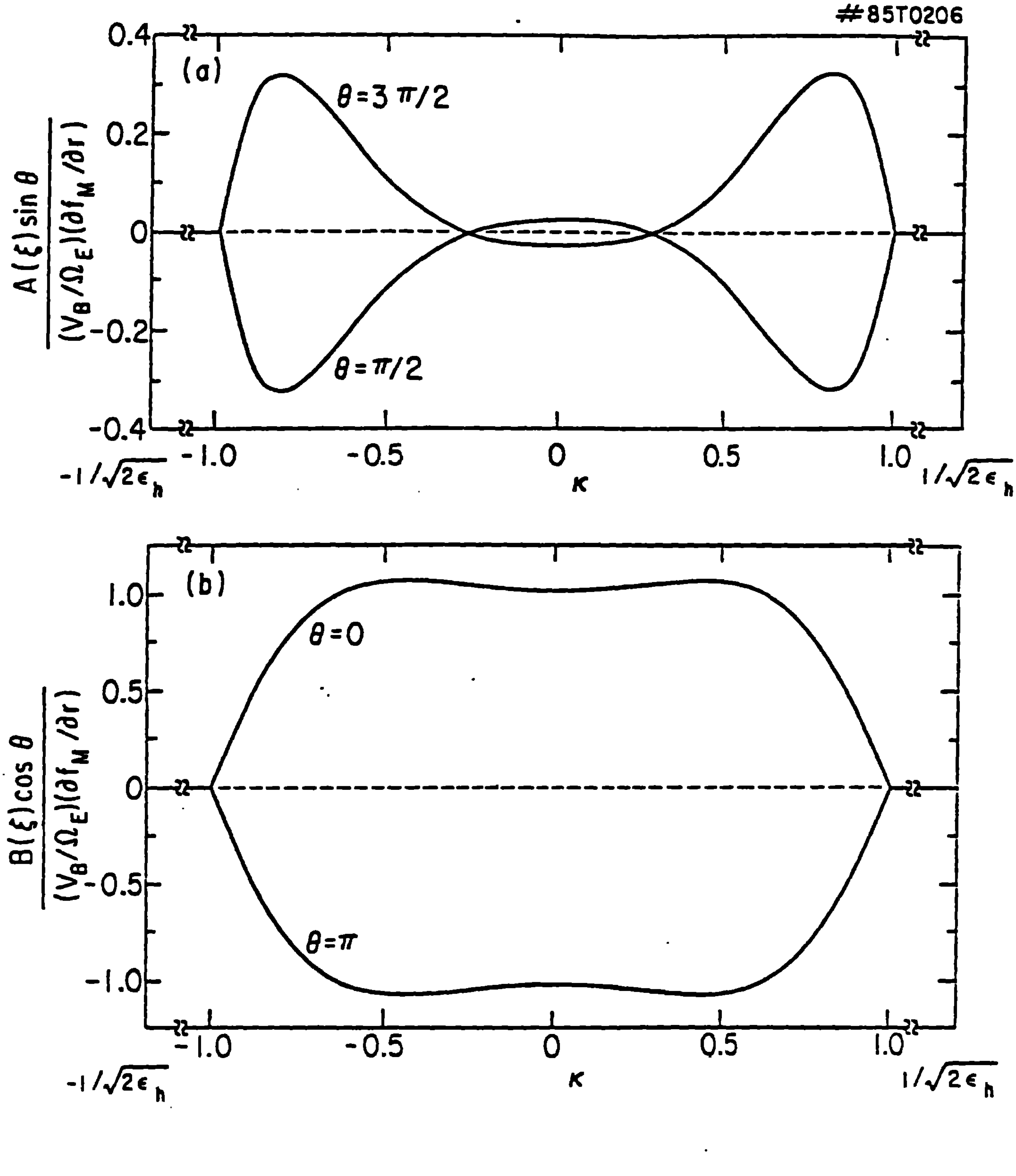
#85T0206
(a)
$\theta=3\pi/2$
$\theta=\pi/2$
$\frac{A(\xi)\sin\theta}{(V_B/\Omega_E)(\partial f_M/\partial r)}$
0.4
0.2
0
-0.2
-0.4
$-1/\sqrt{2\epsilon_h}$
-1.0
-0.5
0
0.5
1.0
$1/\sqrt{2\epsilon_h}$
κ
(b)
$\theta=0$
$\theta=\pi$
$\frac{B(\xi)\cos\theta}{(V_B/\Omega_E)(\partial f_M/\partial r)}$
1.0
0.5
0
-0.5
-1.0
$-1/\sqrt{2\epsilon_h}$
-1.0
-0.5
0
0.5
1.0
$1/\sqrt{2\epsilon_h}$
κ

Fig. 6

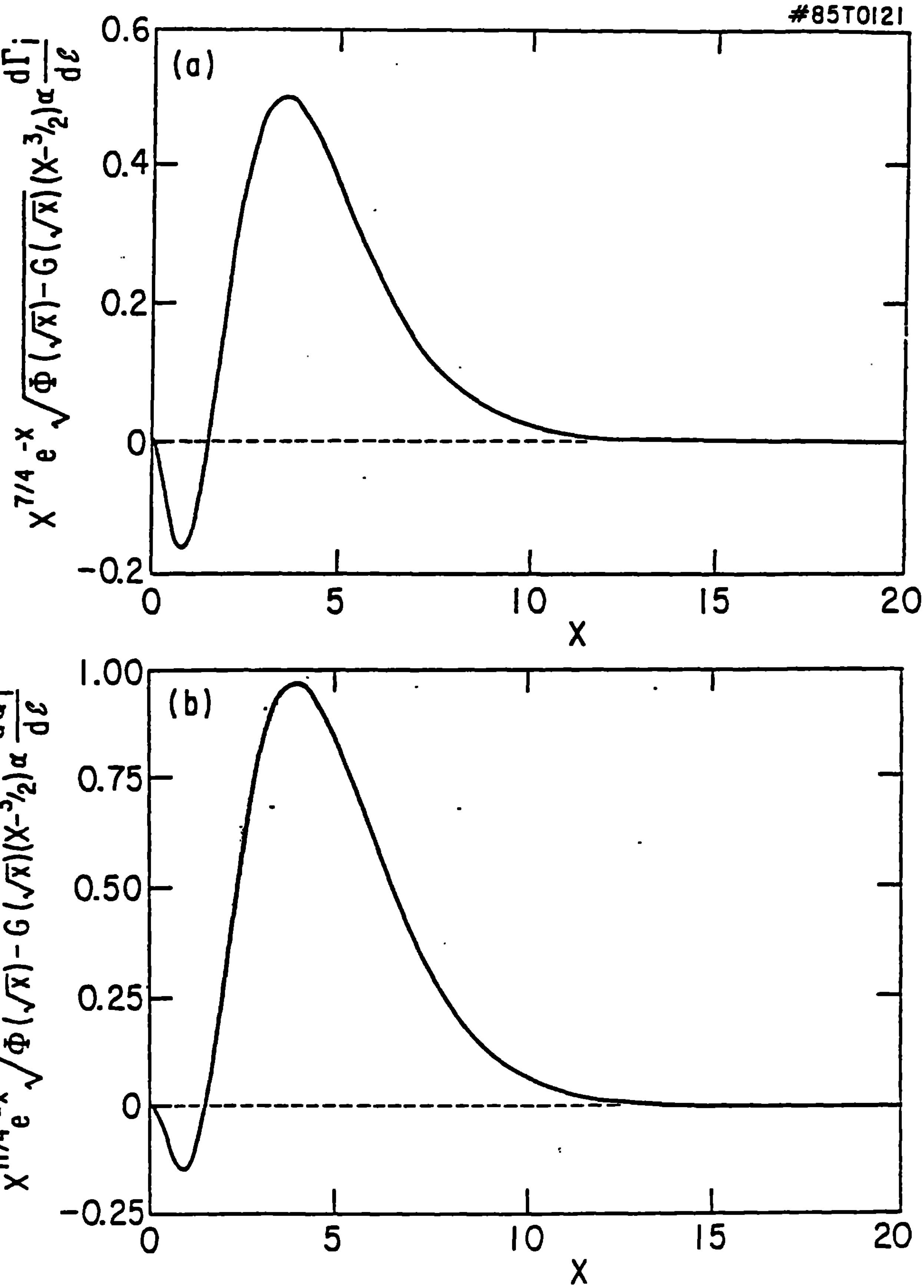
#85T0121
(a)
$X^{7/4} e^{-X} \sqrt{\Phi(\sqrt{X}) - G(\sqrt{X})}\,(X - 3/2)\,\alpha \frac{d\Gamma_i}{d\mathcal{E}}$
0.6
0.4
0.2
0
−0.2
0
5
10
15
20
X
(b)
$X^{11/4} e^{-X} \sqrt{\Phi(\sqrt{X}) - G(\sqrt{X})}\,(X - 3/2)\,\alpha \frac{dQ_i}{d\mathcal{E}}$
1.00
0.75
0.50
0.25
0
−0.25
0
5
10
15
20
X

Fig. 7

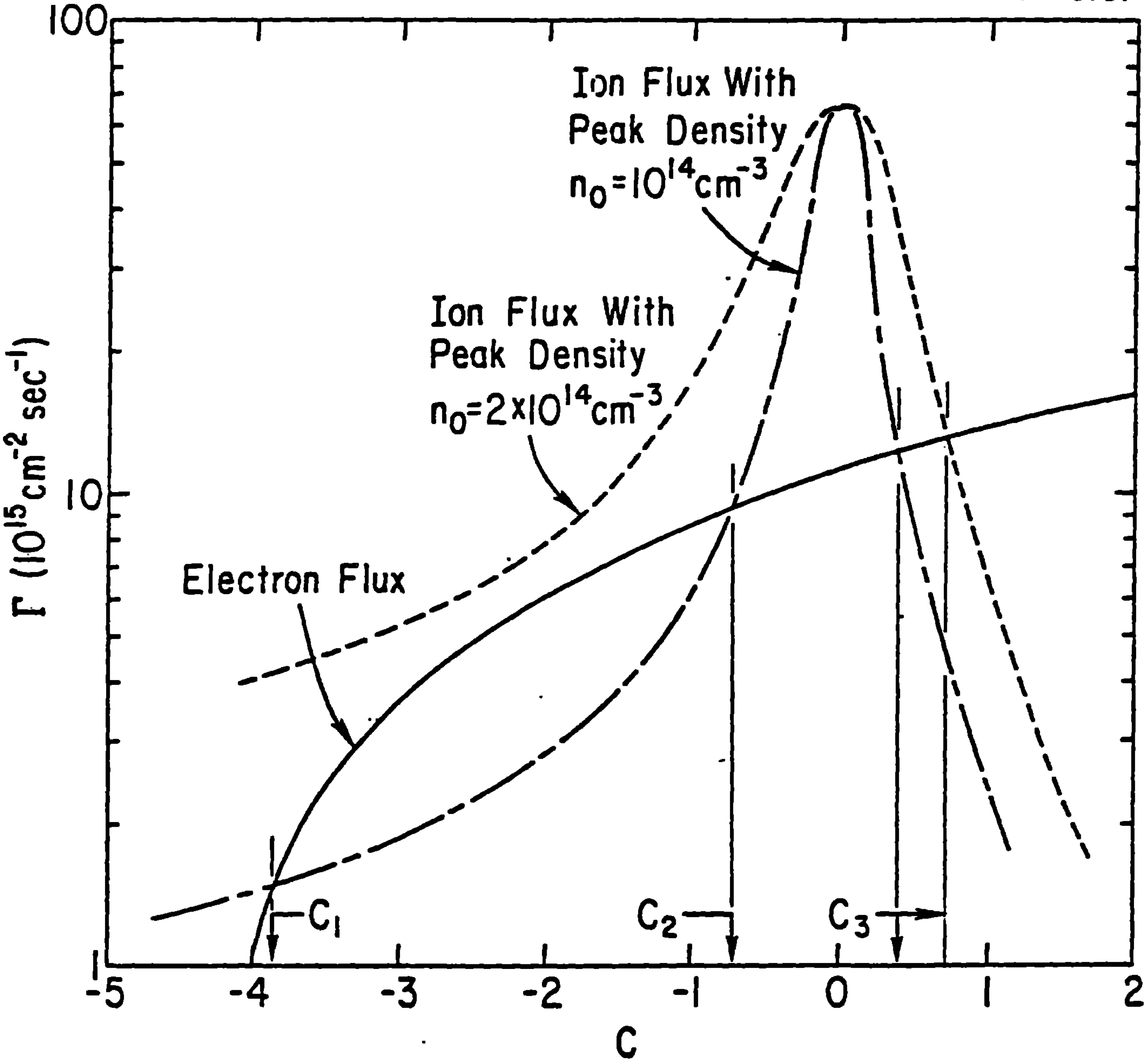
Ion Flux With
Peak Density
$n_0=10^{14}cm^{-3}$
Ion Flux With
Peak Density
$n_0=2\times10^{14}cm^{-3}$
Electron Flux
$\Gamma\ (10^{15}cm^{-2}\ sec^{-1})$
100
10
1
-5
-4
-3
-2
-1
0
1
2
C
C_1
C_2
C_3

Fig. 8

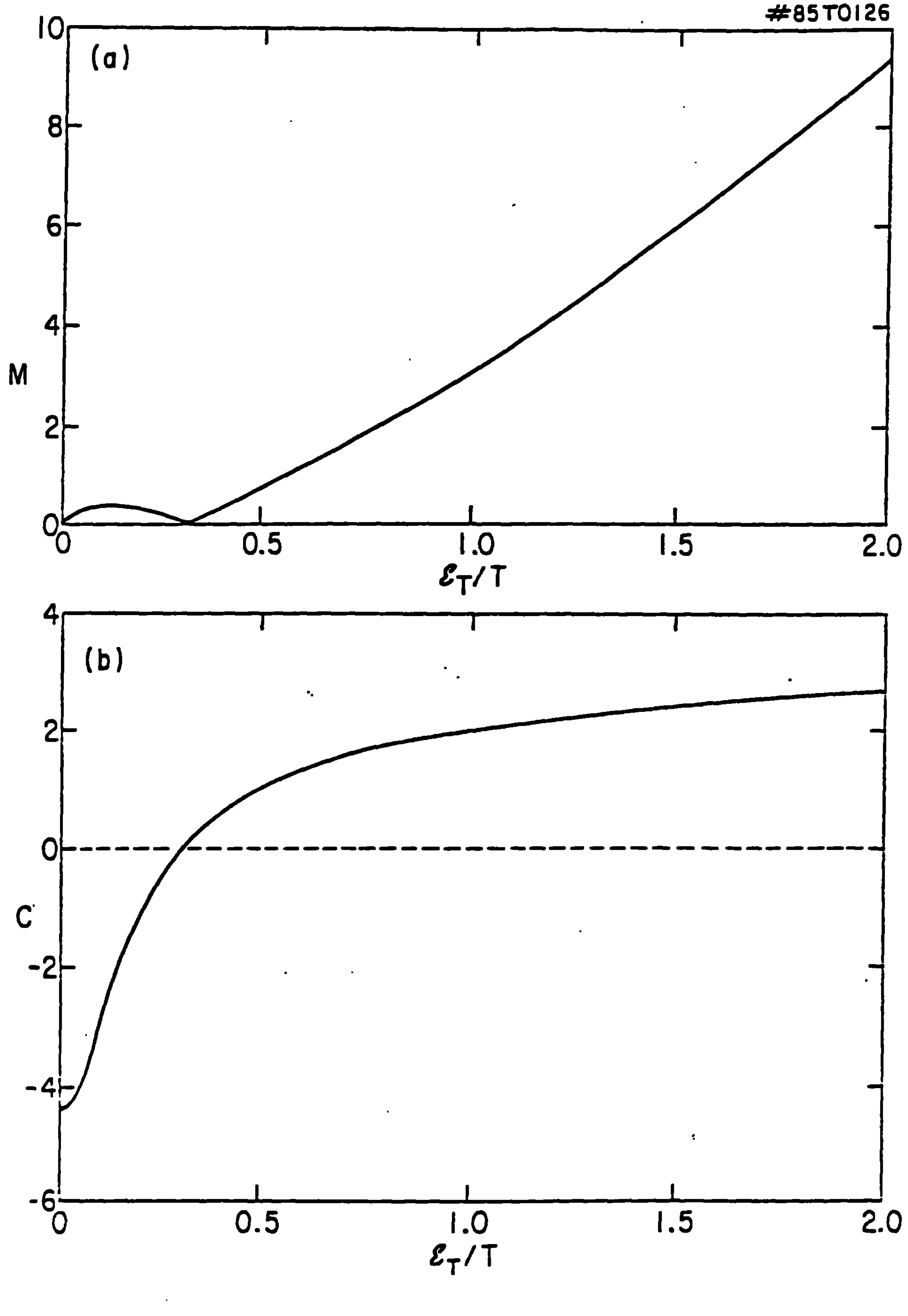
#85T0126
(a)
M
10
8
6
4
2
0
0
0.5
1.0
1.5
2.0
$\mathcal{E}_T/T$
(b)
C
4
2
0
-2
-4
-6
0
0.5
1.0
1.5
2.0
$\mathcal{E}_T/T$

Fig. 9

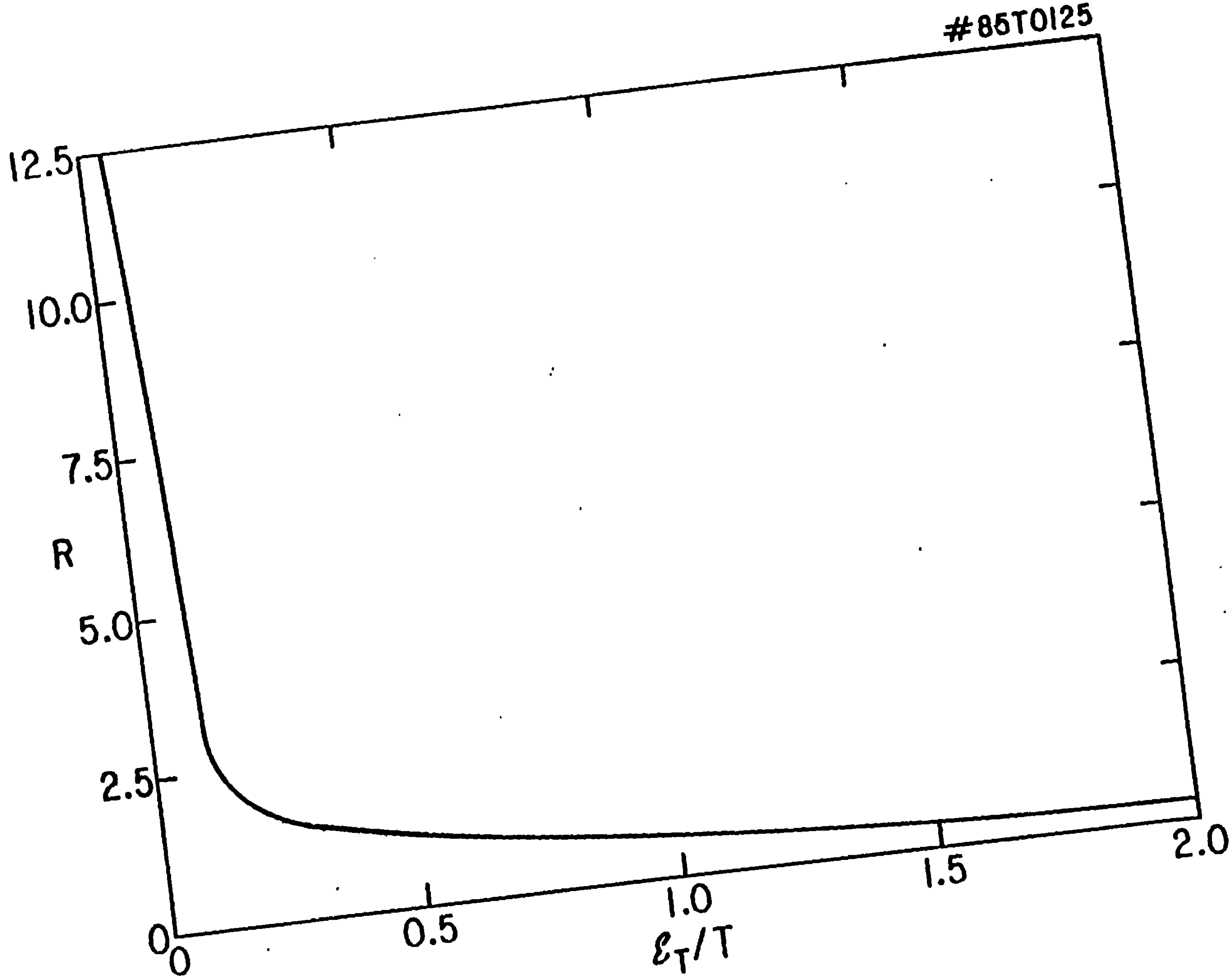

Fig. 10

#85T0177

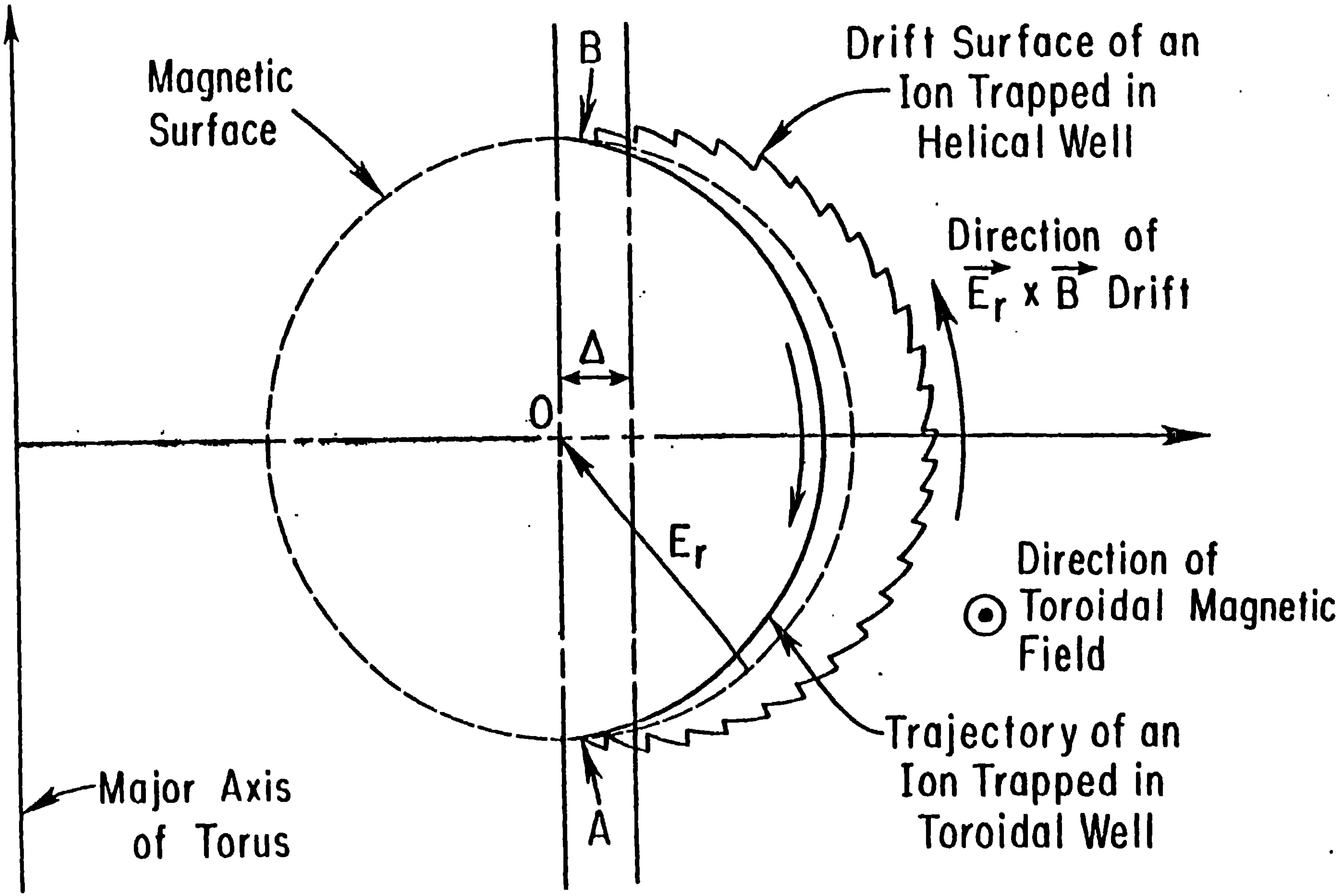

Fig. 11